

Neutrinoless double-beta decay in a finite volume from relativistic effective field theory

Y. L. Yang¹ and P. W. Zhao^{1,*}

¹*State Key Laboratory of Nuclear Physics and Technology,
School of Physics, Peking University, Beijing 100871, China*

arXiv:2407.19695v3 [nucl-th] 2 Nov 2024

Abstract

The neutrinoless double-beta decay process $nn \rightarrow ppee$ within the light Majorana-exchange scenario is studied using the relativistic pionless effective field theory (EFT) in finite-volume cubic boxes with the periodic boundary conditions. Using the low-energy two-nucleon scattering observables from lattice QCD available at $m_\pi = 300, 450, 510,$ and 806 MeV, the leading-order $nn \rightarrow ppee$ transition matrix elements are predicted and their volume dependence is investigated. The predictions for the $nn \rightarrow ppee$ transition matrix elements can be directly compared to the lattice QCD calculations of the $nn \rightarrow ppee$ process at the same pion masses. In particular for the matrix element at $m_\pi = 806$ MeV, the predictions with relativistic pionless EFT are confronted to the recent first lattice QCD evaluation. Therefore, the present results are expected to play a crucial role in the benchmark between the nuclear EFTs and the upcoming lattice QCD calculations of the $nn \rightarrow ppee$ process, which would provide a nontrivial test on the predictive power of nuclear EFTs on neutrinoless double-beta decay.

I. INTRODUCTION

Neutrinoless double-beta decay ($0\nu\beta\beta$) is a second-order weak process, where a nucleus decays to its neighboring nucleus by turning two neutrons to two protons, emitting two electrons but no corresponding antineutrinos [1]. It violates the lepton number conservation of the Standard Model (SM) of particle physics and, if observed, would confirm that neutrinos are of Majorana nature [2, 3]. The theoretical calculations of the $0\nu\beta\beta$ decay rate, combined with experimental searches [4–11], will advance our knowledge of beyond-Standard-Model (BSM) mechanisms that may be responsible for this process. Moreover, the theoretical predictions of the expected decay rate in the given BSM scenarios will benefit the planned experiments on $0\nu\beta\beta$ [12]. However, the theoretical calculations so far suffer from considerable uncertainties, which hamper the interpretation of current experimental limits on $0\nu\beta\beta$ and potential future discoveries.

A major source of uncertainty in calculating the $0\nu\beta\beta$ decay rate is the nuclear matrix elements between the initial and final nuclear states. For the isotopes of experimental interest for $0\nu\beta\beta$ searches, such uncertainties stem from both the approximations in nuclear-structure

* pwzhao@pku.edu.cn

models used to solve the many-body wave function, as well as the uncertainties in the $0\nu\beta\beta$ decay operator [13]. The latter can be singled out by studying the amplitude of $0\nu\beta\beta$ decay in the two-nucleon sector, i.e., $nn \rightarrow ppee$, since the two-body wave function can be accurately solved in this case. Although the $nn \rightarrow ppee$ transition is not observed in the free space, it occurs as the key subprocess in the $0\nu\beta\beta$ decay in nuclei.

Nuclear effective field theories (EFTs) play an important role in addressing the uncertainties of nuclear matrix elements. Depending on the energy regime of interest, the nuclear EFTs include the chiral EFT [14, 15], designed for momenta of the order of the pion mass m_π , and the pionless EFT [16–21], which focuses on momenta well below m_π (For recent reviews, see Refs. [22–24]). Based on a power-counting scheme, they can provide an order-by-order routine to improve the $0\nu\beta\beta$ decay operator, which can then be used as inputs in nuclear-structure calculations. The $0\nu\beta\beta$ decay operators derived from the nuclear EFTs under various BSM scenarios [25–33], as well as their impacts on the nuclear matrix elements [34–40], have been extensively studied in the literature. Here, we focus on the widely considered BSM scenario, the light Majorana-neutrino exchange [41]. At leading order (LO), according to the Weinberg power counting of chiral EFT, the only contribution to the $0\nu\beta\beta$ decay operator comes from the long-range neutrino exchange [27]. However, in the nonrelativistic heavy-baryon formulation, a renormalization-group analysis showed that a $nn \rightarrow ppee$ contact term should be promoted to LO to ensure renormalizability [28, 29]. The low-energy constant (LEC) of this contact term is so far highly uncertain because it can only be fixed by fitting to lepton-number-violating data, currently unavailable. Subsequently, a synthetic datum of the $nn \rightarrow ppee$ amplitude is proposed by developing a generalized Cottingham formula [31, 32]. Nevertheless, this approach introduces model-dependent inputs for elastic intermediate states and neglects inelastic contributions, and the resulting uncertainties need to be further scrutinized.

In contrast to the nonrelativistic formulation, it was recently found that the uncertain $nn \rightarrow ppee$ contact term is not required at LO in the relativistic formulation of chiral EFT [33]. This formulation is similar to the so-called modified Weinberg approach [42] developed for two-nucleon scattering, proven to be useful to improve the renormalizability of two-nucleon scattering phase shifts [42] and the binding energies of few-body systems [43, 44]. Thanks to the milder ultraviolet behavior of the relativistic scattering equation, the $nn \rightarrow ppee$ amplitude from long-range neutrino exchange is ultraviolet finite and, thus,

can be properly renormalized without promoting the uncertain contact term to the LO decay operator [33]. As a result, the $nn \rightarrow ppee$ amplitudes are predicted in a way that is free of model-dependent inputs beyond the EFT framework and can serve as alternative synthetic data to estimate the LEC of the LO $nn \rightarrow ppee$ contact term in the nonrelativistic formulation. The predicted $nn \rightarrow ppee$ amplitudes from the relativistic chiral EFT are slightly larger, by about 10%-40% than the amplitudes from the generalized Cottingham formula [31], depending on the kinematics. This discrepancy in the amplitudes will in turn propagate to the contact-term contribution in nuclear structure calculations of realistic $0\nu\beta\beta$ decay. Therefore, it is crucial to validate the $nn \rightarrow ppee$ amplitudes obtained by the existing approaches.

A direct way to validate the EFT predictions on the $nn \rightarrow ppee$ amplitudes is to perform first-principles lattice QCD (LQCD) calculations that incorporate the dynamics of quarks and gluons [45–51]. In fact, LQCD has already demonstrated its reach and capability in constraining the pionic amplitudes for the $0\nu\beta\beta$ processes $\pi^-\pi^- \rightarrow ee$ and $\pi^- \rightarrow \pi^+ee$ within the light Majorana-neutrino exchange scenario [52–54] and the $\pi^- \rightarrow \pi^+ee$ process within a heavy-scale scenario [55]. The LQCD calculations of the processes involving two nucleons are more complicated. The LQCD computations for the two-neutrino double beta decay $nn \rightarrow ppee\bar{\nu}_e\bar{\nu}_e$ [56, 57] and, recently, the $0\nu\beta\beta$ decay $nn \rightarrow ppee$ [58] have been achieved. However, these calculations are currently tractable only at unphysical heavy pion masses, due to the computational cost. Therefore, to directly benchmark with the available and upcoming LQCD results of the $nn \rightarrow ppee$ process, the nuclear EFTs need to be implemented at the heavy pion masses same as those in the LQCD calculations.

In addition, the LQCD calculations of the matrix elements are implemented on a finite-volume lattice in Euclidean spacetime, which means that there are no asymptotic states. In contrast, the nuclear EFTs calculate the scattering amplitudes within the infinite volume in Minkowski spacetime. The matching procedure between the Euclidean finite-volume matrix elements and the infinite-volume scattering amplitude for the $nn \rightarrow ppee$ process has been developed [59, 60]. It builds upon the major developments in recent years in accessing transition amplitudes in hadronic physics from the corresponding finite-volume Euclidean matrix elements [61–71] and, in particular, the similar procedure developed for two-neutrino double-beta decay $nn \rightarrow ppee\bar{\nu}_e\bar{\nu}_e$ [72]. First, the connection between the Euclidean matrix element, accessible in LQCD, and its Minkowski counterpart is constructed. Then, the

nonrelativistic formulation of LO pionless EFT is implemented in a finite volume to derive the Minkowski counterpart of the LQCD matrix element. The Minkowski matrix element depends on the LEC of the LO $nn \rightarrow ppee$ contact term in the pionless EFT, whose size is still uncertain. In Ref. [60], this LEC is estimated from the generalized Cottingham formula [31, 32]. However, this estimation is only applicable at the physical pion mass. At the unphysical heavy pion mass tractable in the LQCD calculations, the nonrelativistic pionless EFT needs to fit the LQCD results of the $nn \rightarrow ppee$ matrix elements to fix the unknown LEC of $nn \rightarrow ppee$ contact term, instead of making predictions.

In this work, we implement the relativistic formulation of pionless EFT in a finite volume at various pion masses, to predict the Minkowski matrix elements that can be directly compared to the LQCD calculations of the $nn \rightarrow ppee$ process. Different from the nonrelativistic case, we estimate the LEC of the LO $nn \rightarrow ppee$ contact term by integrating out the pion contributions to the long-range neutrino potential in the relativistic chiral EFT. This is possible because the long-range $nn \rightarrow ppee$ amplitudes are renormalizable in the relativistic chiral EFT [33]. For the physical pion mass, we compare the scattering amplitudes from the relativistic formulation with the previous nonrelativistic results in Ref. [60] with the contact term fixed by the generalized Cottingham formula [31]. For the unphysical pion masses $m_\pi = 300, 450, 510, \text{ and } 806 \text{ MeV}$, using the available two-nucleon observables from the LQCD calculations [73–77] as inputs, we present the EFT predictions of the LO Minkowski matrix elements in finite volumes, as well as the scattering amplitude in the infinite volume. Finally, we compare the EFT predictions and the first LQCD evaluation of matrix element at $m_\pi = 806 \text{ MeV}$ [58] with the same finite volume. The present results can be used in the future benchmarks between the nuclear EFTs and the LQCD calculations of the $nn \rightarrow ppee$ process, which would provide a solid assessment of the predictive power of nuclear EFTs on $0\nu\beta\beta$ decay. The results are also expected to be instructive for the analysis of the systematic uncertainties in the future LQCD calculations of the $nn \rightarrow ppee$ process.

II. THEORETICAL FRAMEWORK

In section II A, we describe the relativistic formulation of pionless EFT [33, 42, 44] employed to evaluate the $nn \rightarrow ppee$ amplitudes. In section II B, we briefly introduce the implementation of the relativistic formulation of pionless EFT in a finite volume, closely

following the derivations in Refs. [59, 60] for the nonrelativistic case.

A. Relativistic formulation of pionless EFT

The pionless EFT is based on the tenet that the few-nucleon processes at very low energies, i.e., $Q \ll m_\pi$, are not sensitive to the details associated with pions or other meson exchanges [24]. Then, all mesons can be integrated out and the effective Lagrangian contains nucleon and lepton degrees of freedom, organized according to the number of derivatives. The observables are expanded in Q/m_π , where Q is the low-energy scale of the order of the binding momentum $\gamma = \sqrt{m_N B_{NN}}$ or of the inverse of the scattering length a . At LO, the effective Lagrangian reads

$$\mathcal{L}_{\Delta L=0} = \bar{\Psi}(i\gamma^\mu \partial_\mu - m_N)\Psi - \sum_\alpha \frac{C_\alpha}{2} (\bar{\Psi}\Gamma_\alpha\Psi)^2 + \frac{1}{2}\bar{\Psi}(l_\mu\gamma^\mu + g_A l_\mu\gamma^\mu\gamma_5)\Psi, \quad (1)$$

with Ψ the nucleon field, m_N the nucleon mass, LECs C_α , $\alpha = S, V, AV, T$, and Γ_α the corresponding Dirac gamma matrices. The nucleons are coupled to the electroweak current l_μ via both vector coupling $g_V = 1$ and axial coupling $g_A = 1.27$. Here, we neglect the dependence of g_A on the unphysical pion mass. This dependence can be easily taken into account once its value is provided by the LQCD calculations at the corresponding pion mass since it only provides constant factors on the neutrino potential. The electroweak current reads $l_\mu = -2\sqrt{2}G_F V_{ud}\tau^+\bar{e}\gamma_\mu\nu_{eL} + \text{h.c.}$, with the Fermi constant G_F and the V_{ud} element of the Cabibbo-Kobayashi-Maskawa (CKM) matrix [78, 79].

After expanding the nucleon field in terms of the free Dirac spinors $u(\mathbf{p}, s)$ with positive energies in momentum space and keeping only the leading term of $u(\mathbf{p}, s)$ expanding in powers of small momenta \mathbf{p} , the LO strong potential takes the following form,

$$V_S(\mathbf{p}', \mathbf{p}) = \frac{m_N}{\omega_{p'}} \frac{m_N}{\omega_p} [C_S + C_V - (C_{AV} - 2C_T)\boldsymbol{\sigma}_1 \cdot \boldsymbol{\sigma}_2], \quad (2)$$

where \mathbf{p}' and \mathbf{p} are the nucleon's final and initial momenta in the center-of-mass frame, respectively, and $\omega_p = (m_N^2 + p^2)^{1/2}$. At the leading order of pionless EFT, the interaction only contributes to the s wave. Here, we consider the 1S_0 channel relevant for the $nn \rightarrow ppee$ process, in which $\boldsymbol{\sigma}_1 \cdot \boldsymbol{\sigma}_2 = -3$, and the LEC $C = C_S + C_V + 3(C_{AV} - 2C_T)$ determines the interaction strength in this channel. As in the nonrelativistic case, the LEC C scales as $\mathcal{O}(4\pi/(m_N Q))$ so that the LO amplitudes consist of a resummation of the LO interaction V_S

and the low-energy pole in the two-nucleon 1S_0 amplitude can be reproduced. In particular, for the two-nucleon scattering process, the amplitude reads

$$i\mathcal{M}_S(E) = -iV_S(p, p) + \int \frac{d^3k}{(2\pi)^3} (-i)V_S(p, k) \frac{i}{E - 2\omega_k + i0^+} i\mathcal{M}_S(E). \quad (3)$$

with $p = \sqrt{\frac{1}{4}E^2 - m_N^2}$. After regularizing the contact term with a separable regulator, $V_S(p', p) \rightarrow V_S(p', p)f_\Lambda(p')f_\Lambda(p)$, with momentum cutoff Λ , the scattering amplitude takes the form

$$\mathcal{M}_S(E) = -\frac{1}{C_\Lambda^{-1} - I_\Lambda(E)}, \quad (4)$$

where the ‘‘bubble integral’’ reads

$$I_\Lambda(E) = \int \frac{d^3k}{(2\pi)^3} \frac{m_N^2}{\omega_k^2} \frac{1}{E - 2\omega_k + i0^+} [f_\Lambda(k)]^2. \quad (5)$$

The divergence of the ‘‘bubble integral’’ is absorbed into the cutoff dependence of the LEC C_Λ and the resulting scattering amplitude is cutoff-independent as $\Lambda \rightarrow \infty$. For the two-nucleon bound state, the energy eigenvalue E and the momentum-space wave function $\phi_E(\mathbf{p})$ are obtained by solving the following eigen equation

$$(E - 2\omega_p)\phi(\mathbf{p}) = \int \frac{d^3k}{(2\pi)^3} V_S(p, k)\phi(\mathbf{k}). \quad (6)$$

Beyond LO, the strong interactions arise from the Lorentz-invariant contact Lagrangian with an increasing number of derivatives (See Ref. [80] for the expressions of the contact Lagrangian up to fourth-order derivatives). Here, we consider the ordering of the contact terms in the relativistic pionless EFT to be the same as its nonrelativistic counterpart, because they both should reproduce the effective range expansion order by order, $p \cot \delta(p) = -\frac{1}{a} + \frac{1}{2}rp^2 \dots$, with the ellipse denoting high-order momentum dependences. The subleading contribution is given by the effective range $r \sim O(m_\pi^{-1})$, and it is of the order $O(Q/m_\pi)$ relative to the LO contribution. Once properly renormalized, the difference between the LO relativistic and nonrelativistic pionless EFTs is that the former includes higher-order terms dictated by the Lorentz invariance. For example, the LO relativistic EFT yields a small effective range of $r \sim O(m_N^{-1})$, while the nonrelativistic theory yields exactly zero effective range $r = 0$.

In this work, we consider the standard mechanism of $0\nu\beta\beta$ decay, in which the lepton number violation at low energies is dominated by a Majorana mass term

$$\mathcal{L}_{\Delta L=2} = -\frac{m_{\beta\beta}}{2} \nu_{eL}^T C \nu_{eL}, \quad (7)$$

where $C = i\gamma_2\gamma_0$ denotes the charge conjugation matrix and $m_{\beta\beta}$ the effective neutrino mass. Following naive dimension analysis, the LO neutrino potential is contributed only by the long-range exchange of a potential neutrino,

$$V_{\nu\text{L}}(\mathbf{p}', \mathbf{p}) = (1 + 3g_A^2) \frac{m_N}{\omega_{p'}} \frac{m_N}{\omega_p} \frac{1}{|\mathbf{p}' - \mathbf{p}|^2}, \quad (8)$$

and its contribution is $O(Q^{-2})$. Similar to the strong potential, there are m_N/ω_p factors coming from the expansion of the nucleon field without performing the nonrelativistic reduction. However, in pionless EFT, it is known that contact operators in weak processes are typically enhanced when S waves are involved [24, 81]. This leads to the existence of a contact term in the LO neutrino potential—despite being expected two orders down in the naive dimension analysis

$$V_{\nu\text{CT}}(\mathbf{p}', \mathbf{p}) = -2 \frac{m_N}{\omega_{p'}} \frac{m_N}{\omega_p} g_\nu^{NN}. \quad (9)$$

with g_ν^{NN} the corresponding LEC. However, different from the nonrelativistic case, g_ν^{NN} does not serve as a counterterm that absorbs the ultraviolet divergence, since the LO long-range amplitude itself is ultraviolet finite [33]. As a result, the contact-term contribution to the LO amplitude is finite in relativistic pionless EFT and can be estimated by integrating out the pion contributions in the relativistic chiral EFT, as we will demonstrate below.

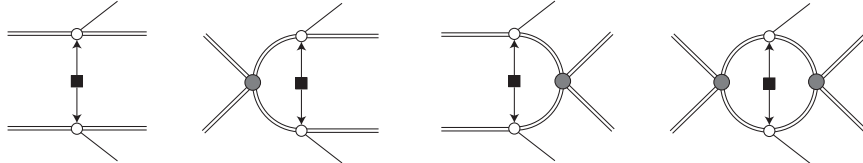


FIG. 1. Diagrams contributing to the LO long-range $nn \rightarrow ppee$ amplitude. The amplitude $\mathcal{M}_{0\nu}^{(\text{int})}$ excluding neutrino exchanges on the external legs is shown by the last diagram. The double and plain lines denote nucleons and leptons, respectively. The squares denote insertions of neutrino potential V_ν . The empty circles denote the nucleon axial and vector currents coupled to neutrino exchange. The gray circles represent the LO two-nucleon scattering amplitude \mathcal{M}_S .

The LO long-range $nn \rightarrow ppee$ amplitude can be schematically written as

$$\mathcal{M}_{0\nu,\text{L}} = -m_{\beta\beta}(1 + 3g_A^2) (V_{\nu\text{L}} - \mathcal{M}_S I^\infty - \bar{I}^\infty \mathcal{M}_S + \mathcal{M}_S J^\infty \mathcal{M}_S), \quad (10)$$

with \mathcal{M}_S is the LO two-nucleon scattering amplitude [Eq. (4)], and I^∞ and J^∞ are the one- and two-loop integrals with a neutrino exchange. Here, the four terms correspond to the four

diagrams depicted in Fig. 1. The first three terms are the contributions in which a neutrino propagates between two external nucleons. The last term, where a neutrino propagates between two nucleons dressed by strong interactions in both the initial and final states, is the subject of matching to LQCD matrix elements [59],

$$\mathcal{M}_{0\nu,L}^{(\text{int})}(E_f, E_i) = -m_{\beta\beta}(1 + 3g_A^2)\mathcal{M}_S(E_f)J^\infty(E_f, E_i)\mathcal{M}_S(E_i), \quad (11)$$

where J^∞ takes the form,

$$J^\infty(E_f, E_i) = \int \frac{d^3k_1}{(2\pi)^3} \frac{d^3k_2}{(2\pi)^3} \frac{m_N^2}{\omega_{k_1}^2} \frac{1}{E_f - 2\omega_{k_1} + i0^+} \frac{m_N^2}{\omega_{k_2}^2} \frac{1}{E_i - 2\omega_{k_2} + i0^+} \frac{1}{|\mathbf{k}_1 - \mathbf{k}_2|^2}. \quad (12)$$

This two-loop integral is ultraviolet finite in the present relativistic formulation, but divergent in the nonrelativistic case. This is because, in the nonrelativistic approach, the $1/m_N$ expansion is carried out for the integrand making its ultraviolet behavior more singular and resulting in a logarithmic divergence.

Now, we discuss the contact-term contribution to the LO $nn \rightarrow ppee$ amplitude. It is well known that the coupling of the axial current to pions gives rise to the Goldberg-Treiman relation between the pseudoscalar and axial contribution to the weak form factor. In the relativistic chiral EFT, this effect is included in the LO long-range neutrino potential,

$$\delta V_{\nu L}(\mathbf{p}', \mathbf{p}) = -g_A^2 \frac{m_N}{\omega_{p'}} \frac{m_N}{\omega_p} \frac{|\mathbf{p}' - \mathbf{p}|^2 + 2m_\pi^2}{(|\mathbf{p}' - \mathbf{p}|^2 + m_\pi^2)^2}, \quad (13)$$

while in the relativistic pionless EFT, the contributions from $\delta V_{\nu L}$ are integrated out and will manifest in the form of a contact term. Therefore, the LO contact term g_ν^{NN} can be estimated by the contribution of $\delta V_{\nu L}$. This is achieved by inserting $\delta V_{\nu L}$ into the four diagrams in Fig. 1 and considering m_π as a hard scale. The first tree-level diagram is just $\delta V_{\nu L} \sim O(m_\pi^{-2})$, i.e., next-to-next-to-leading order (NNLO). The contribution of the second diagram can be written as $-g_A^2 \delta I_\pi^\infty(E_f, E_i)\mathcal{M}_S(E_i)$ with $\delta I_\pi^\infty(E_f, E_i)$ the one loop integral with an insertion of $\delta V_{\nu L}$,

$$\delta I^\infty(E_f, E_i) = \int \frac{d^3k}{(2\pi)^3} \frac{m_N^2}{\omega_k^2} \frac{1}{E_f - 2\omega_k + i0^+} \frac{|\mathbf{k} - \mathbf{p}_i|^2 + 2m_\pi^2}{(|\mathbf{k} - \mathbf{p}_i|^2 + m_\pi^2)^2}. \quad (14)$$

Expanding this integral around the threshold $E_f = E_i = 0$, we have $\delta I^\infty(E_f, E_i) = \delta I^\infty(0, 0) + O(Q^2/m_\pi^2)$. Then, $I_\pi^\infty(0, 0)$ is just a function of the hard scales m_π and M , and dimension analysis determines $\delta I^\infty(E_f, E_i) \sim O(m_N/(4\pi m_\pi))$. Since the scaling of \mathcal{M}_S is $O(4\pi/(m_N Q))$, the contribution of second diagram is subleading, $O((m_\pi Q)^{-1})$. Following

the above analysis, the contribution of the third diagram is also subleading, $O((m_\pi Q)^{-1})$, but the contribution of the fourth diagram is instead LO, $O(Q^{-2})$. The latter takes the form

$$\delta\mathcal{M}_{0\nu}^{(\text{int})}(E_f, E_i) = m_{\beta\beta}g_A^2\mathcal{M}_S(E_f)\delta J^\infty(E_f, E_i)\mathcal{M}_S(E_i) \quad (15)$$

with

$$\delta J^\infty(E_f, E_i) = \int \frac{d^3k_1}{(2\pi)^3} \frac{d^3k_2}{(2\pi)^3} \frac{m_N^2}{\omega_{k_1}^2} \frac{1}{E_f - 2\omega_{k_1} + i0^+} \frac{m_N^2}{\omega_{k_2}^2} \frac{1}{E_i - 2\omega_{k_2} + i0^+} \frac{|\mathbf{k}_1 - \mathbf{k}_2|^2 + 2m_\pi^2}{(|\mathbf{k}_1 - \mathbf{k}_2|^2 + m_\pi^2)^2}. \quad (16)$$

This two-loop integral has a mass dimension of two and thus scales as $O(m_N^2/(4\pi)^2)$. As a result, $\delta\mathcal{M}_{0\nu}^{(\text{int})}(E_f, E_i) \sim O(Q^{-2})$ and needs to be accounted for by a LO contact term. The contact term contributes to the amplitude as

$$\mathcal{M}_{0\nu, \text{CT}}^{(\text{int})}(E_f, E_i) = 2m_{\beta\beta}\tilde{g}_\nu^{NN} \left(\frac{m_N}{4\pi}\right)^2 \mathcal{M}_S(E_f)\mathcal{M}_S(E_i) \quad (17)$$

after defining the dimensionless LEC \tilde{g}_ν^{NN} ,

$$\tilde{g}_\nu^{NN} = \left(\frac{4\pi}{m_N C}\right)^2 g_\nu^{NN}. \quad (18)$$

By matching Eqs. (15) and (17) at the threshold $E_f = E_i = 0$, the dimensionless LEC can be determined,

$$\tilde{g}_\nu^{NN} = \frac{(4\pi)^2}{2m_N^2} g_A^2 \delta J^\infty(0, 0). \quad (19)$$

In addition to the contribution originating from the coupling of pions, there could be other unknown short-range contributions to the LO LEC \tilde{g}_ν^{NN} in the relativistic pionless EFT. By comparing the pionless and chiral EFT amplitudes, the unknown short-range contributions in the pionless EFT corresponds to the \tilde{g}_ν^{NN} contact-term contribution in the chiral EFT. It then follows that, based on Weinberg power counting, \tilde{g}_ν^{NN} contribution is expected to be suppressed by two orders in the chiral expansion, i.e., $O(Q^2/\Lambda_\chi^2)$ with $\Lambda_\chi \sim m_N$ the break down scale of chiral EFT. Based on this estimation, the uncertainty of the estimation by Eq. (19) can be considered subleading, since $Q^2/m_N^2 \lesssim Q/m_\pi$ when $m_\pi \leq 806$ MeV (see Table I).

Finally, adding up the long-range and contact-term contributions, the amplitude is given by

$$\mathcal{M}_{0\nu}^{(\text{int})}(E_f, E_i) = -m_{\beta\beta}\mathcal{M}_S(E_f) \left[(1 + 3g_A^2)J^\infty(E_f, E_i) - 2\tilde{g}_\nu^{NN} \left(\frac{m_N}{4\pi}\right)^2 \right] \mathcal{M}_S(E_i). \quad (20)$$

B. Implementation in a finite volume

In this work, we implement the relativistic pionless EFT in a finite-volume (FV) cubic box with spatial extent L and the periodic boundary conditions. Considering the $nn \rightarrow ppee$ process with the kinematics that the two electrons in the final state are at rest, the Euclidean four-point function accessible from LQCD can be analytically continued to the Minkowski spacetime [59],

$$\mathcal{T}_L^{(M)}(E_f, E_i) = \int dz_0 \int_L d^3z [\langle E_f, L | T[\mathcal{J}(z_0, \mathbf{z}) S_\nu(z_0, \mathbf{z}) \mathcal{J}(0)] | E_i, L \rangle]_L, \quad (21)$$

where the subscript L on the spatial integral indicates that the integral is performed over the FV cubic box and $|E, L\rangle$ is the normalized FV s -wave two-nucleon state with the center-of-mass energy E . Here, \mathcal{J} denotes the hadronic part of the weak current, and the neutrino propagator $S_\nu(z_0, \mathbf{z})$ in a finite volume is given by the Fourier transformation

$$S_\nu(z_0, \mathbf{z}) = \frac{1}{L^3} \sum_{\substack{\mathbf{q} \in \frac{2\pi}{L}\mathbb{Z}^3 \\ \mathbf{q} \neq \mathbf{0}}} \int \frac{dq_0}{2\pi} e^{i\mathbf{q} \cdot \mathbf{z} - iq_0 z_0} \frac{-im_{\beta\beta}}{q_0^2 - \mathbf{q}^2 + i0^+}, \quad (22)$$

ignoring the small nonzero neutrino mass. Because the space is limited to a box with the periodic boundary conditions, the momentum modes are discretized, only taking the values with $2\pi/L$ times three-dimensional Cartesian vectors with integer components. The infrared divergence is regulated by removing the zero-momentum mode of neutrinos.

The energy eigenvalues of the two-nucleon states are also discretized in a finite volume. Their discrete values E_n are directly related to the two-nucleon scattering amplitudes in the infinite volume, by the Lüscher quantization condition $\mathcal{F}^{-1}(E_n) = 0$ [82, 83]. For the 1S_0 channel considered in this work, it is

$$\mathcal{F}^{-1}(E) = \frac{4\pi}{m_N} \left(-\frac{1}{\pi L} \mathcal{Z}_{00} \left[1, \left(\frac{pL}{2\pi} \right)^2 \right] + ip \right)^{-1} + \mathcal{M}_S(E), \quad (23)$$

where \mathcal{Z}_{00} is the zeta function defined in Ref. [82] and $\mathcal{M}_S(E)$ is the scattering amplitude defined in Eq. (4).

For the case in which the initial and final states are “scattering” states, the Minkowski matrix element $\mathcal{T}_L^{(M)}$ is calculated as following [59],

$$L^6 |\mathcal{T}_L^{(M)}(E_f, E_i)|^2 = |\mathcal{R}(E_f)| |\mathcal{M}_{0\nu}^{(\text{int}, L)}(E_f, E_i)|^2 |\mathcal{R}(E_i)|, \quad (24)$$

where two FV quantities $\mathcal{M}_{0\nu}^{(\text{int},L)}$ and \mathcal{R} are involved. The former one corresponds to the amplitude (Eq. 20) in a finite volume [59, 60],

$$\mathcal{M}_{0\nu}^{(\text{int},L)}(E_f, E_i) = -m_{\beta\beta}\mathcal{M}_S(E_f) \left[(1 + 3g_A^2)J^L(E_f, E_i) - 2\tilde{g}_\nu^{NN} \left(\frac{m_N}{4\pi} \right)^2 \right] \mathcal{M}_S(E_i). \quad (25)$$

The function J^L resembles the function J^∞ in the infinite volume [Eq. (12)], with the momentum integrals replaced by the sum of discrete momentum modes,

$$J^L(E_f, E_i) = \frac{1}{L^6} \sum_{\substack{\mathbf{k}_1, \mathbf{k}_2 \in \frac{2\pi}{L}\mathbb{Z}^3 \\ \mathbf{k}_1 \neq \mathbf{k}_2}} \frac{m_N^2}{\omega_{k_1}^2} \frac{1}{E_f - 2\omega_{k_1}} \frac{m_N^2}{\omega_{k_2}^2} \frac{1}{E_i - 2\omega_{k_2}} \frac{1}{|\mathbf{k}_1 - \mathbf{k}_2|^2}. \quad (26)$$

Here, the imaginary part of the propagator is dropped since now the denominator takes nonzero discrete values. The FV quantity $\mathcal{R}(E)$ is the generalized Lellouch-Lüscher residue matrix [61],

$$\mathcal{R}(E_n) = \lim_{E \rightarrow E_n} (E - E_n) \mathcal{F}(E) = \left(\frac{d\mathcal{F}^{-1}}{dE} \Big|_{E=E_n} \right)^{-1}, \quad (27)$$

which is the residue of the FV function \mathcal{F} (23) at FV energies E_n .

For the case in which the initial and final states are bound states, $E = 2M - B$ with $B > 0$, the Minkowski matrix element $\mathcal{T}_L^{(M)}$ is calculated by

$$\begin{aligned} \mathcal{T}_L^{(M)}(E_f, E_i) &= m_{\beta\beta} \frac{1}{L^6} \sum_{\substack{\mathbf{k}_1, \mathbf{k}_2 \in \frac{2\pi}{L}\mathbb{Z}^3 \\ \mathbf{k}_1 \neq \mathbf{k}_2}} \phi_{E_f, L}^*(\mathbf{k}_1) V_{\nu L}(\mathbf{k}_1, \mathbf{k}_2) \phi_{E_i, L}(\mathbf{k}_2) \\ &\quad - 2m_{\beta\beta} \tilde{g}_\nu^{NN} \left(\frac{MB}{4\pi} \right)^2 |\phi(\mathbf{0})|^2. \end{aligned} \quad (28)$$

with $\phi_{E, L}(\mathbf{k})$ the normalized momentum-space wave function of the FV state $|E, L\rangle$ in Eq. (21). On the right hand side, the first and the second terms are respectively the expectations of the long-range neutrino potential $V_{\nu L}$ in Eq. (8) and the contact term in Eq. (9) regulated with the same separable regulator as the one for the strong interaction. The wave function $\phi_{E, L}$ is solved by Eq. (6) with discrete momentum modes. Although there is no two-nucleon bound state in the 1S_0 channel at the physical pion mass, the above matrix element is relevant for the study at the unphysical pion masses. At the unphysical pion masses, two nucleons might exhibit a 1S_0 bound state predicted by the LQCD calculations [73–76]. Note that there is an ongoing discussion on whether such a bound state exists at the unphysical pion masses, as several newer works [77, 84–86] do not identify such a bound state.

III. NUMERICAL DETAILS

In this work, we consider several box sizes in the range of $L = 8\text{-}16$ fm at the physical pion mass, and $L = 4\text{-}6$ fm at the unphysical pion masses in accordance with the existing LQCD calculations of two-nucleon systems [73–76]. We focus on the scattering amplitudes and the FV matrix elements with equal initial and final energies, $E_f = E_i = E$. This neglects the masses of the two electrons in the final state of the $nn \rightarrow ppee$ process, since they are much smaller than the intervals between the discrete FV energies. Throughout this work, the effective neutrino mass $m_{\beta\beta}$ is set to 1 MeV. For the LO strong potential, we use an exponential regulator $f_\Lambda(k) = e^{-k^4/\Lambda^4}$.

A. Calculations in the infinite volume

The momentum integrals (5), (12), (6) associated with the calculations in the infinite volume are all calculated numerically using Gaussian quadrature. For the calculations of the scattering amplitudes, the real and imaginary parts of the two-nucleon free propagator are calculated separately,

$$\frac{1}{E - 2\omega_k + i0^+} = P\left(\frac{1}{E - 2\omega_k}\right) - i\pi\delta(E - 2\omega_k). \quad (29)$$

Here, P denotes principle-value integral and it is eliminated by a standard subtraction technique [87]. The eigen equation (6) for the bound states is solved by matrix diagonalization on the Gaussian grids.

However, special care has to be taken for the infrared singularity of the neutrino potential. For the calculation of the scattering amplitude $\mathcal{M}_{0\nu}^{(\text{int})}$, inserting the separation (29) into the expression of the two-loop integral J^∞ (12), we have

$$\begin{aligned} \text{Re}J^\infty(E_f, E_i) = & \int_0^\infty \frac{k_1^2 dk_1}{2\pi^2} \left[\frac{m_N^2}{\omega_{k_1}^2} P\left(\frac{1}{E_f - 2\omega_{k_2}}\right) \int_0^\infty \frac{k_2^2 dk_2}{2\pi^2} \right. \\ & \left. \frac{m_N^2}{\omega_{k_2}^2} P\left(\frac{1}{E_i - 2\omega_{k_2}}\right) \frac{1}{4k_1 k_2} \ln \frac{(k_1 + k_2)^2}{(k_1 - k_2)^2} \right] - \frac{m_N^2}{32\pi^2} \frac{m_N}{\omega_{p_f}} \frac{m_N}{\omega_{p_i}} \ln \frac{p_f + p_i}{|p_f - p_i|}. \end{aligned} \quad (30)$$

On the right-hand side, there are logarithmic divergences in the two terms when $E_f = E_i$. We introduce a subtraction technique making use of the analytic expression of the following

two-loop integral,

$$\begin{aligned}
I_\Lambda^\infty &= \int_0^\Lambda \frac{k_1^2 dk_1}{2\pi^2} P\left(\frac{1}{E_f - k_1^2/m_N}\right) \int_0^\infty \frac{k_2^2 dk_2}{2\pi^2} P\left(\frac{1}{E_i - k_2^2/m_N}\right) \frac{1}{4k_1 k_2} \ln \frac{(k_1 + k_2)^2}{(k_1 - k_2)^2} \\
&= \frac{m_N^2}{32\pi^2} \ln \frac{\Lambda^2 - p_i^2}{|p_f^2 - p_i^2|}.
\end{aligned} \tag{31}$$

Denoting the integral term in Eq. (30) as I^∞ , then we have

$$\text{Re}J^\infty(E_f, E_i) = \left(I^\infty - \frac{m_N^2}{\omega_{p_f} \omega_{p_i}} I_\Lambda^\infty \right) + \frac{m_N^2}{\omega_{p_f} \omega_{p_i}} \frac{m_N^2}{32\pi^2} \ln \frac{\Lambda^2 - p_i^2}{(p_f + p_i)^2} \tag{32}$$

Now, the two terms are both infrared convergent when $E_f = E_i$ and we have confirmed the numerical stability using the above expression.

For the calculations of the matrix element $\mathcal{T}_L^{(M)}$ between bound states, the infrared singularity of the neutrino potential is treated with the Lande subtraction [88–91],

$$\int_0^\infty \frac{dk}{2\pi^2} \frac{1}{4kp} \ln \frac{(k+p)^2}{(k-p)^2} k^2 f(k) = \int_0^\infty \frac{dk}{2\pi^2} \frac{1}{4kp} \ln \frac{(k+p)^2}{(k-p)^2} [k^2 f(k) - p^2 f(p)] + \frac{1}{8} p f(p) \tag{33}$$

with $f(p)$ an arbitrary smooth function.

B. Calculations in a finite volume

For the calculations of the matrix elements $\mathcal{T}_L^{(M)}$ between the “scattering” states, the FV quantity J^L (26), which involves summation over the discrete three-momenta $\mathbf{k}_1, \mathbf{k}_2 = \mathbf{n}2\pi/L$ with $\mathbf{n} \in \mathbb{Z}^3$, is calculated using the method of tail-singularity separation (TSS) described in Ref. [92]. In this method, the summation is split into two pieces. One piece contains the singular contributions around $\mathbf{k}_1 = \mathbf{k}_2$, but it is exponentially decaying when $|\mathbf{k}_1|, |\mathbf{k}_2| \rightarrow \infty$. The other piece contains a power-law decaying tail at $|\mathbf{k}_1|, |\mathbf{k}_2| \rightarrow \infty$, but it is sufficiently smooth so that it can be approximated by its integral counterpart. Based on this method, we calculate J^L as the following

$$\begin{aligned}
J^L(E, E) &= \frac{m_N^2}{4(2\pi)^6} \left\{ \sum_{\mathbf{n}_1 \in \mathbb{Z}^3} \frac{\tilde{m}}{\tilde{m}^2 + n_1^2} \frac{1}{\tilde{\omega}_{n_1} - \tilde{\omega}_p} \left[\mathcal{X}_{\text{sum}}(\mathbf{n}_1, \tilde{p}^2) + e^{-\alpha(n_1^2 - \tilde{p}^2)} \mathcal{X}_{\text{int}}(n_1^2, \tilde{p}^2) \right] \right. \\
&\quad \left. + 4\pi \int_0^\infty n_1^2 dn_1 \frac{\tilde{m}}{\tilde{m}^2 + n_1^2} \frac{1 - e^{-\alpha(n_1^2 - \tilde{p}^2)}}{\tilde{\omega}_{n_1} - \tilde{\omega}_p} \mathcal{X}_{\text{int}}(n_1^2, \tilde{p}^2) \right\} + O(e^{-\pi^2/\alpha}),
\end{aligned} \tag{34}$$

where $\tilde{m} = 2\pi m_N/L$, $\tilde{p} = 2\pi p/L$, $\tilde{\omega} = (\tilde{m}^2 + \tilde{p}^2)^{1/2}$, and

$$\begin{aligned}\mathcal{X}_{\text{sum}}(\mathbf{n}_1, \tilde{p}^2) &= \sum_{\substack{\mathbf{n}_2 \in \mathbb{Z}^3 \\ \mathbf{n}_2 \neq \mathbf{n}_1}} \frac{\tilde{m}}{\tilde{m}^2 + n_2^2} \frac{1}{\tilde{\omega}_{n_2} - \tilde{\omega}_p} \frac{1}{|\mathbf{n}_1 - \mathbf{n}_2|^2} \left[1 - (1 - e^{-\alpha(n_2^2 - \tilde{p}^2)})(1 - e^{-\alpha|\mathbf{n}_1 - \mathbf{n}_2|^2}) \right] \\ \mathcal{X}_{\text{int}}(n_1^2, \tilde{p}^2) &= \int d^3 n_2 \frac{\tilde{m}}{\tilde{m}^2 + n_2^2} \frac{1 - e^{-\alpha(n_2^2 - \tilde{p}^2)}}{\tilde{\omega}_{n_2} - \tilde{\omega}_p} \frac{1 - e^{-\alpha|\mathbf{n}_1 - \mathbf{n}_2|^2}}{|\mathbf{n}_1 - \mathbf{n}_2|^2} - \alpha \frac{\tilde{m}}{\tilde{m}^2 + n_1^2} \frac{1 - e^{-\alpha(n_1^2 - \tilde{p}^2)}}{\tilde{\omega}_{n_1} - \tilde{\omega}_p}.\end{aligned}\tag{35}$$

In the expression of \mathcal{X}_{int} , the second term removes the value at the pole $\mathbf{n}_2 = \mathbf{n}_1$ when replacing $\sum_{\mathbf{n}_2} \rightarrow \int d^3 n_2$. We use $\alpha = 0.01$ and truncate the integer Cartesian coordinates at $|n_x|, |n_y|, |n_z| \leq 32$ in the present calculations. Under this condition, we evaluate the geometric constants \mathcal{X}_2 with a single sum and \mathcal{R}_{24} with double sums, as defined in Eq. (A1) of Ref. [93], by using the TSS method. We obtain $\mathcal{X}_2 = 91.18$ and $\mathcal{R}_{24} = 170.9$, which agrees with the corresponding results of Ref. [93] up to four significant figures.

For the calculations of the matrix element $\mathcal{T}_L^{(M)}$ between the bound states, they can be straightforwardly calculated using Eq. (28), once the bound-state wave function $\phi_{E,L}$ is solved. When solving the bound-state wave function, we truncate the integer sum at $|n_x|, |n_y|, |n_z| \leq \Lambda L/(2\pi)$. The number of momentum modes could reach several thousand, making direct diagonalization intractable. Therefore, we use the imaginary-time propagation starting from an initial wave function ϕ_i to solve for the bound-state wave function

$$\phi_{E,L} = \lim_{N\tau \rightarrow \infty} (e^{-H\Delta\tau})^{N\tau} \phi_i,\tag{36}$$

where $\Delta\tau$ is a small imaginary-time step, and $e^{-H\Delta\tau}$ is expanded up to $O(\Delta\tau^2)$. This is particularly efficient because of the separable form of the potential,

$$H\phi(\mathbf{p}) = 2\omega_p\phi(\mathbf{p}) + C_\Lambda f_\Lambda(p^2) \frac{1}{L^3} \sum_{\mathbf{k} \in \frac{2\pi}{L}\mathbb{Z}^3} f_\Lambda(k^2)\phi(\mathbf{k}),\tag{37}$$

so the numerical complexity scales linearly with the number of momentum modes, instead of cubically when using direct diagonalization. We take the initial wave function to be $\phi_i(\mathbf{p}) = e^{-p^2/m_N^2}$, but using a different form should not affect the final results once the imaginary-time projection converges.

C. Determination of low-energy constants

At the leading order of relativistic pionless EFT, there are two LECs C_Λ and \tilde{g}_ν^{NN} that need to be determined for predicting the scattering amplitudes and matrix elements for the

TABLE I. The nucleon masses m_N and the two-nucleon binding energies B_{nn} in the 1S_0 channel at $m_\pi = 300, 450, 510,$ and 806 . The LEC C_Λ for the LO strong potential, determined at $\Lambda = 50$ fm^{-1} using these inputs, are shown in the fourth column. The LEC \tilde{g}_ν^{NN} for the LO $nn \rightarrow ppee$ contact term, determined by Eq. (19), are shown in the last column. The uncertainty of \tilde{g}_ν^{NN} from the LQCD inputs is smaller than the last digit and thus not shown. At the physical pion mass, since no 1S_0 bound state exists, the LEC C_Λ is instead fixed by the scattering length $a = -23.74$ fm. At $m_\pi = 806$ MeV, two sets of LQCD inputs are considered (see text for details).

m_π (MeV)	m_N (MeV)	B_{nn} (MeV)	C_Λ (fm^2)	\tilde{g}_ν^{NN}
140	938.9	-	-0.4157	1.66
300 [75]	1055(4)	$8.5^{(+1.7)}_{(-0.9)}$	$-0.3666^{(+14)}_{(-24)}$	1.20
450 [76]	1226(2)	$13.1^{(+3.0)}_{(-3.1)}$	$-0.2875^{(+29)}_{(-25)}$	1.03
510 [73]	1320(3)	$7.4(1.4)$	$-0.2483^{(+15)}_{(-14)}$	1.00
806 [74]	1634(18)	$15.9(3.8)$	$-0.1780^{(+19)}_{(-17)}$	0.85
806* [77]	1636(18)	$3.3(7)$	$-0.1585^{(+40)}_{(-31)}$	0.85

$nn \rightarrow ppee$ process. For C_Λ , it is the strength of the short-range strong potential and can be fixed by one low-energy observable in the 1S_0 channel. The observables used to determine C_Λ are shown in Table I. At the physical pion mass, there is no 1S_0 bound state, so we fix it using the experimental scattering length $a = -23.74$ fm. At the unphysical pion masses, several LQCD calculations yielded deeply bound 1S_0 two-nucleon state [73–76]. However, many other LQCD studies [77, 85, 86, 94, 95] did not obtain such bound states, raising concerns on whether or not the previous works correctly determined the two-nucleon spectrum. There are several explanations for this issue and it is still not completely conclusive whether 1S_0 two-nucleon state is bound or unbound at unphysical large pion masses [96]. Nevertheless, the results from the present work could be easily adjusted to updated LQCD values of two-nucleon binding energies or scattering lengths. For example, in Table I, we considered both the older (without asterisk) [74] and the latest (with asterisk) [77] LQCD values of B_{nn} at $m_\pi = 806$ MeV. For $m_\pi = 300, 400, 510,$ and 806 MeV, the LEC C_Λ is fixed using the two-nucleon binding energy B_{nn} in the infinite volume, extrapolated from the FV energies provided by the LQCD calculations. For $m_\pi = 806^*$ MeV, the LQCD result of B_{nn} is only available at a single finite volume $L = 4.6$ fm and, thus, the fitting of the LEC C_Λ is

performed at the same finite volume.

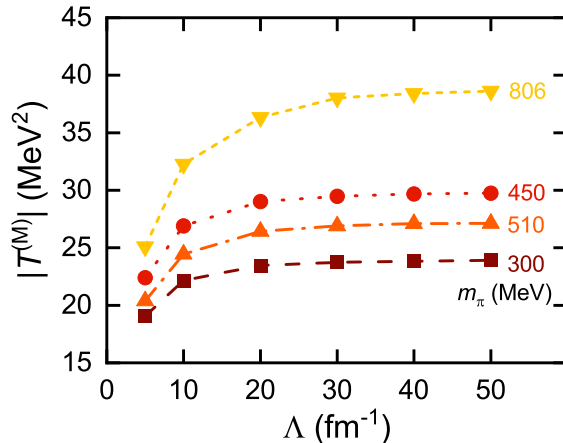


FIG. 2. (Color online). The cutoff dependence of the long-range contribution to the LO Minkowski matrix elements $\mathcal{T}^{(M)}$ for the ground-state-to-ground-state transitions in the infinite volume at the pion masses $m_\pi = 300, 450, 510,$ and 806 MeV, obtained from the relativistic pionless EFT. Here, the effective neutrino mass $m_{\beta\beta}$ is set to 1 MeV.

In Fig. 2, we show the cutoff dependence of the long-range contribution to the LO Minkowski matrix elements between the ground states in the infinite volume, $\mathcal{T}^{(M)} = \langle E_0 | V_\nu | E_0 \rangle$, at the unphysical pion masses. Here, the LEC C_Λ is fitted to the center value of B_{nn} in Table I. As expected, the long-range contribution to the matrix elements all converge as the cutoff Λ goes to infinity. For the unphysical pion masses considered here, convergence can be reached at $\Lambda \lesssim 50$ fm $^{-1}$ on the 1% level. As shown in Ref. [33], this is also true for the amplitudes at the physical pion mass. Therefore, we take the amplitudes and matrix elements at $\Lambda = 50$ fm $^{-1}$ as the renormalized results in the present study. The values of LEC C_Λ are listed in Table I.

For the LEC \tilde{g}_ν^{NN} in the LO contact term in the neutrino potential, it is determined by integrating out the contribution from the coupling of the nucleonic axial current to pions, using Eq. 19. They are also calculated from the m_π and m_N values provided by the experiments or LQCD calculations. The values of LEC \tilde{g}_ν^{NN} are listed in Table I. Their values are indeed $O(1)$, as expected. They take positive values and, thus, the contact term contribution reduces the magnitude of the $nn \rightarrow ppee$ amplitude.

IV. RESULTS AND DISCUSSION

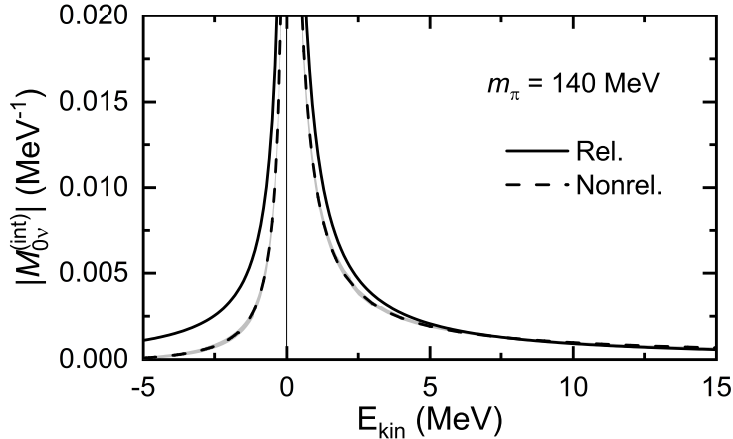


FIG. 3. The amplitudes $|\mathcal{M}_{0\nu}^{(\text{int})}|$ at the physical pion mass obtained from the relativistic and nonrelativistic LO pionless EFT, as functions of the center-of-mass kinetic energy $E_{\text{kin}} = E - 2m_N$ in the initial and final states. For the nonrelativistic results, the $nn \rightarrow ppee$ contact term is fitted to the synthetic datum provided by the generalized Cottingham formula [31]. The effective neutrino mass $m_{\beta\beta}$ is set to 1 MeV.

We first discuss the $nn \rightarrow ppee$ amplitudes at the physical pion mass. In Fig. 3, the absolute value of the infinite-volume amplitude $\mathcal{M}_{0\nu}^{(\text{int})}$ is plotted against the center-of-mass kinetic energy $E_{\text{kin}} = E - 2m_N$. The amplitudes obtained from the relativistic formulation are compared to those obtained from the nonrelativistic formulation. For the latter, dimensional regularization scheme is adopted to regularize the ultraviolet divergence, introducing the renormalization scale $\mu = m_\pi$, and the LEC for the $nn \rightarrow ppee$ contact term is fitted to the synthetic datum provided by the generalized Cottingham formula [31], yielding $\tilde{g}_\nu^{NN}(\mu = m_\pi) = 4.09 \pm 0.21$. For the energy above the threshold, the nonrelativistic results are consistent with the relativistic ones at 20% level. For the energy under the threshold, the relative difference between the nonrelativistic and relativistic results grows with decreasing energy. The amplitude under the threshold is not observable in the continuum, as the kinetic energy cannot be negative. Nevertheless, it can show up in the matching to the LQCD results, because energies can go below the threshold in finite volumes (e.g., see Fig. 4).

Figure 4 depicts the volume dependence of the FV quantity $\mathcal{M}_{0\nu}^{(\text{int},L)}$ obtained from the relativistic pionless EFT. The FV energies of the ground and first-excited states are shown

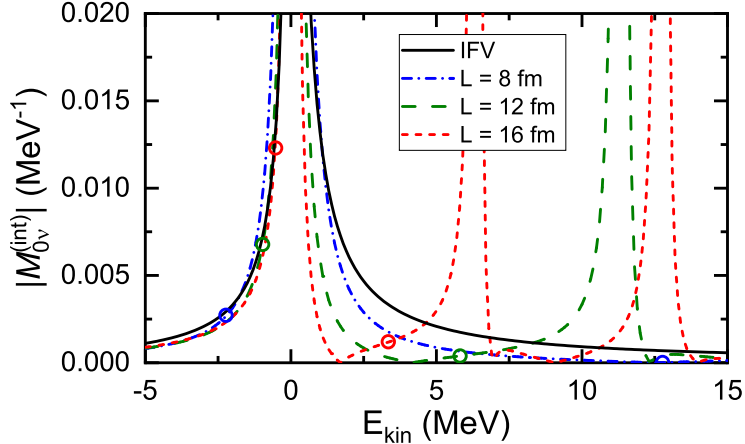


FIG. 4. (Color online). The finite-volume quantities $|\mathcal{M}_{0\nu}^{(\text{int},L)}|$ at the physical pion mass obtained from the LO relativistic pionless EFT, as functions of the center-of-mass kinetic energy $E_{\text{kin}} = E - 2m_N$ in the initial and final states. The infinite-volume (IFV) amplitude $|\mathcal{M}_{0\nu}^{(\text{int})}|$ is shown by the solid line. The empty circles denote the values of $|\mathcal{M}_{0\nu}^{(\text{int},L)}|$ at the finite-volume energies of the ground states and the first excited states. The effective neutrino mass $m_{\beta\beta}$ is set to 1 MeV.

by the empty circles. The infinite-volume amplitude $\mathcal{M}_{0\nu}^{(\text{int})}$ is also shown for comparison. For the energy above the threshold $E_{\text{kin}} > 0$, $\mathcal{M}_{0\nu}^{(\text{int},L)}$ exhibits several singularities in contrast to its infinite-volume counterpart $\mathcal{M}_{0\nu}^{(\text{int})}$. The singularities come from the two-nucleon propagator in Eq. (26), as its denominator becomes zero for the momentum modes in which two nucleons are on-shell, $E_{\text{kin}} = 2\sqrt{m_N^2 + (2\pi\mathbf{n}/L)^2} - 2m_N$ with $\mathbf{n} \in \mathbb{Z}^3$. They do not exist in the infinite volume because the on-shell momentum modes contribute to the imaginary part of the propagator instead of being divergent [see Eq. (12)]. In between the singularities, the value of $\mathcal{M}_{0\nu}^{(\text{int},L)}$ is generally smaller its infinite-volume counterpart $\mathcal{M}_{0\nu}^{(\text{int})}$.

For the energy below the threshold $E_{\text{kin}} < 0$, $\mathcal{M}_{0\nu}^{(\text{int},L)}$ behaves smoothly as a function of energy. In the limit of $L \rightarrow \infty$, the values of $\mathcal{M}_{0\nu}^{(\text{int},L)}$ should approach the infinite-volume amplitude $\mathcal{M}_{0\nu}^{(\text{int})}$. For the range $L = 16$ fm, $\mathcal{M}_{0\nu}^{(\text{int},L)}$ is already close to $\mathcal{M}_{0\nu}^{(\text{int})}$ within 10% at the FV ground-state energies.

Next, we show the results for the matrix elements at the unphysical pion masses $m_\pi = 300, 450, 510, \text{ and } 806$ MeV. In these cases, a two-nucleon bound state in the 1S_0 channel at each pion mass is predicted by the LQCD calculations [73–77]. Figure 5 depicts the volume dependence of the two-nucleon binding energies B_{nn} and the LO Minkowski matrix elements

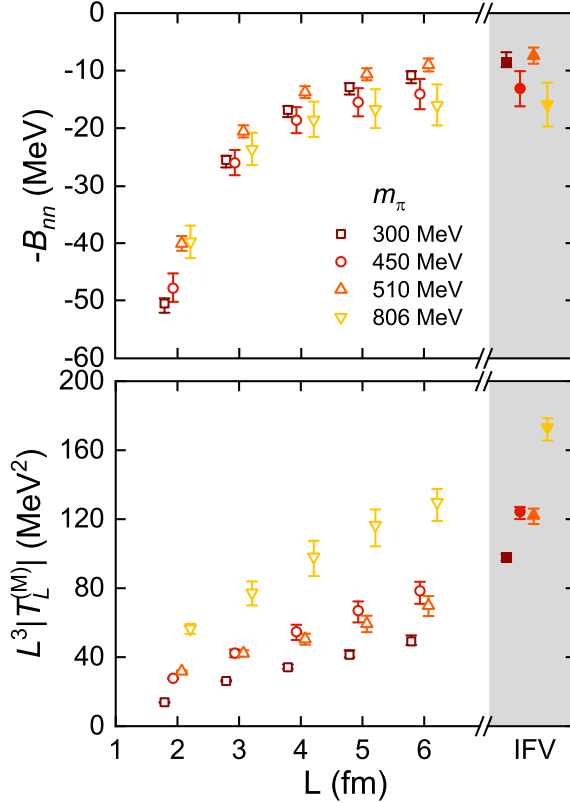


FIG. 5. (Color online). The volume dependence of the two-nucleon binding energies B_{nn} and the LO Minkowski matrix elements $\mathcal{T}_L^{(M)}$ for the ground-state-to-ground-state $nn \rightarrow ppee$ transition at the pion masses $m_\pi = 300, 450, 510,$ and 806 MeV, obtained from the LO relativistic pionless EFT. The results are calculated at integer values of L and slightly shifted in the horizontal direction for clarity. Their infinite-volume (IFV) limits are also shown for comparison. The error bars are obtained by varying the input data of the two-nucleon binding energies B_{nn} from the LQCD calculations within their margins of errors. The effective neutrino mass $m_{\beta\beta}$ is set to 1 MeV.

$\mathcal{T}_L^{(M)}$ for the ground-state-to-ground-state $nn \rightarrow ppee$ transition, as well as their infinite-volume limits. The factor L^3 is added for $\mathcal{T}_L^{(M)}$ to give the correct normalization in the infinite-volume limit $L \rightarrow \infty$. The Minkowski matrix element generally decreases when the pion mass becomes smaller.

For each pion mass, the binding energy B_{nn} becomes significantly large for small box sizes $L \lesssim 3$ fm and comes close to the infinite-volume value at $L = 6$ fm. However, this is not the case for the $nn \rightarrow ppee$ matrix element. At the heaviest pion mass $m_\pi = 806$ MeV,

it increases from 33% of the infinite-volume limit at $L = 2$ fm to 75% at $L = 6$ fm. At the lightest pion mass $m_\pi = 300$ MeV, it increases from 14% of the infinite-volume limit at $L = 2$ fm to only 50% at $L = 6$ fm. The value of $L^3\mathcal{T}_L^{(M)}$ increases slowly with increasing box size, so a much larger box size is needed to approach the infinite-volume limit.

The different volume dependence between the binding energy and the $nn \rightarrow ppee$ matrix element is due to the fact that the strong interaction is short-range while the neutrino exchange is long-range. The photon exchange responsible for the electromagnetic interactions is also long-range, and it is known that the FV corrections for the electromagnetic interactions exhibit a power-law scaling with volume [97], instead of an exponential scaling for the short-range strong interactions. Besides approaching the infinite-volume limit by increasing the box size, one could also extrapolate the results obtained using relatively small box sizes. We extrapolate the values of $L^3\mathcal{T}_L^{(M)}$ at $L = 4, 5, 6$ fm to infinite volume by considering the leading $O(1/L)$ correction. The extrapolation reduces the difference against the infinite-volume limit, but systematic deviation remains. At the heaviest pion mass $m_\pi = 806$ MeV, the extrapolated result overestimates the infinite-volume value by about 10%. While at the lightest pion mass $m_\pi = 300$ MeV, the extrapolated result underestimates the infinite-volume value by about 20%.

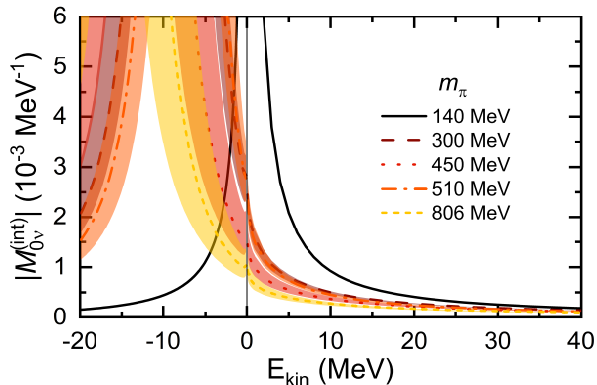


FIG. 6. (Color online). The amplitudes $|\mathcal{M}_{0\nu}^{(\text{int})}|$ at different pion masses obtained from the LO relativistic pionless EFT, as functions of the center-of-mass kinetic energy $E_{\text{kin}} = E - 2m_N$ in the initial and final states. The shaded uncertainties are obtained by varying the input data of the two-nucleon binding energies B_{nn} from the LQCD calculations within their margins of errors. The effective neutrino mass $m_{\beta\beta}$ is set to 1 MeV.

Figure 6 depicts the absolute value of the amplitude $\mathcal{M}_{0\nu}^{(\text{int})}$ at different pion masses. The

shaded uncertainties are obtained by varying the input data from the LQCD calculations within their margins of errors. For the energy above the threshold, the amplitudes $|\mathcal{M}_{0\nu}^{(\text{int})}|$ at the unphysical pion masses are significantly smaller than that at the physical pion mass. $|\mathcal{M}_{0\nu}^{(\text{int})}|$ drops rapidly with increasing energy, which is similar at both the physical and unphysical masses.

For the energy below the threshold, however, the amplitude $|\mathcal{M}_{0\nu}^{(\text{int})}|$ exhibits very different behavior at the unphysical pion masses compared to that at the physical pion mass. In particular, the amplitude $|\mathcal{M}_{0\nu}^{(\text{int})}|$ diverges at the energy of two-nucleon bound state at each unphysical pion mass, because the bound-state energy is the pole of the two-nucleon scattering amplitude $M_S(E)$. For the $nn \rightarrow ppee$ transition between bound states, the scattering amplitude $|\mathcal{M}_{0\nu}^{(\text{int})}|$ (and also $|\mathcal{M}_{0\nu}^{(\text{int},L)}|$) is not well-defined and one should directly calculate the Minkowski matrix element $\mathcal{T}^{(M)}$ ($\mathcal{T}_L^{(M)}$) using bound-state wave functions. Such divergence does not exist at the physical pion mass since there is no two-nucleon bound state in the 1S_0 channel.

In Fig. 7, the FV quantities $|\mathcal{M}_{0\nu}^{(\text{int},L)}|$ at the unphysical pion masses with the box sizes $L = 4, 5, 6$ fm are depicted in comparison with the results in the infinite volume, as functions of the center-of-mass kinetic energy above the threshold. Here, the results are obtained using the central values of LEC in Table I and the uncertainties from the LQCD inputs are not shown. The behavior of $|\mathcal{M}_{0\nu}^{(\text{int},L)}|$ at the unphysical pion masses are similar to that at the physical pion mass except for the locations of singularities. This is because $|\mathcal{M}_{0\nu}^{(\text{int},L)}|$ diverges at the neighborhood of the integer multiples of $4\pi^2/(L^2m_N)$, at which the two nucleons can become on-shell in the FV two-loop integral J^L [Eq. (26)]. As a result, the singularities are denser at heavier pion mass, since the nucleon mass increases with increasing pion mass, and for larger spatial volumes. The FV energies of the ground states and the first excited states in the different spatial volumes are shown by the empty circles. The values of $|\mathcal{M}_{0\nu}^{(\text{int},L)}|$ at the FV energies are significantly smaller than the infinite-volume amplitude $|\mathcal{M}_{0\nu}^{(\text{int})}|$.

In Table II, we provide the values of the LO Minkowski matrix elements $\mathcal{T}_L^{(M)}$ for the ground-state-to-ground-state and first-excited-state-to-first-excited-state $nn \rightarrow ppee$ transitions in finite volumes with $L = 4, 5,$ and 6 fm. The precision of the predicted matrix elements is mostly within 10%-20%. This precision is in accordance with the precision of the two-nucleon binding energies B_{nn} from the LQCD calculations (Table I) used as inputs. In addition to the uncertainty from the LQCD input, there are also uncertainties from the

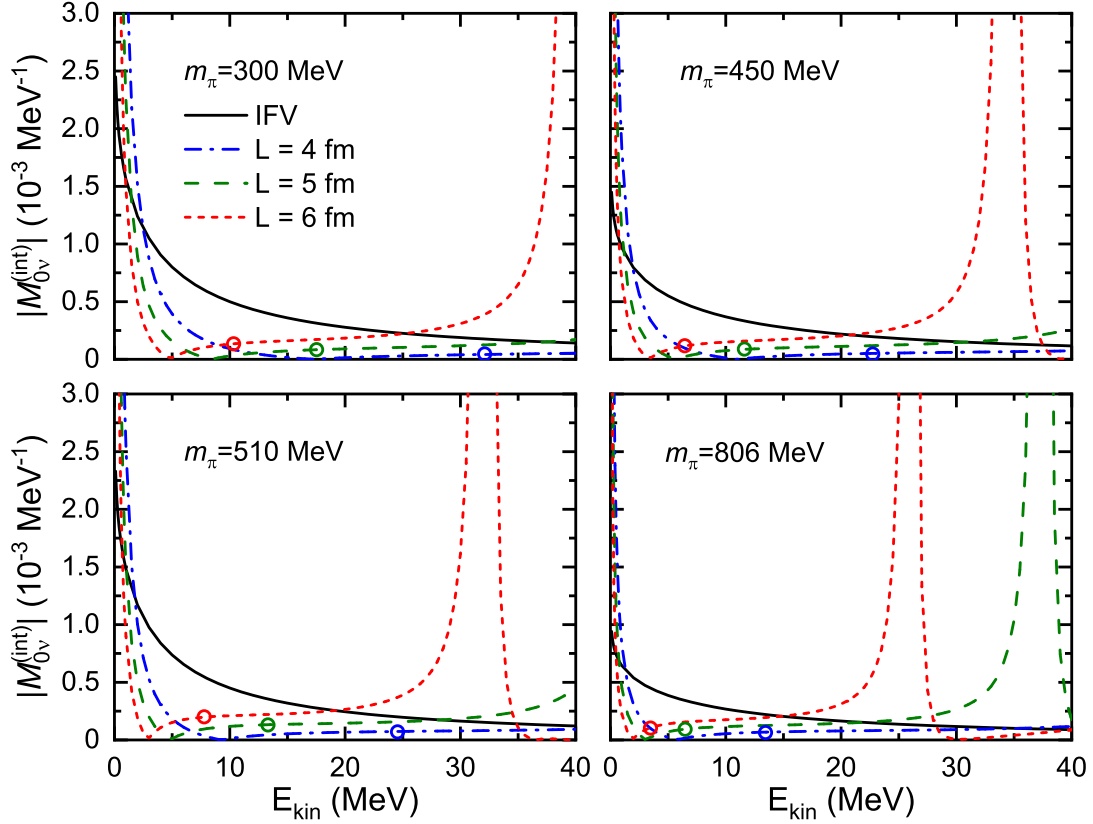


FIG. 7. (Color online). The finite-volume quantities $|\mathcal{M}_{0\nu}^{(\text{int},L)}|$ at the unphysical pion masses obtained from the LO relativistic pionless EFT, as functions of the center-of-mass kinetic energy $E_{\text{kin}} = E - 2m_N$ in the initial and final states. The empty circles denote the values of $|\mathcal{M}_{0\nu}^{(\text{int},L)}|$ at the finite-volume energies of the ground states and the first excited states. The infinite-volume (IFV) amplitudes $|\mathcal{M}_{0\nu}^{(\text{int})}|$ are also shown by the solid lines. Here, the results are obtained using the central values of the two-nucleon binding energies B_{nn} from the LQCD calculations as inputs. The effective neutrino mass $m_{\beta\beta}$ is set to 1 MeV.

truncation of EFT and the estimation of the LO LEC \tilde{g}_{ν}^{NN} , as discussed in Sec. II A. For the former, the uncertainty arises from neglecting the strong potential and neutrino potential beyond LO, expected to be $O(Q/m_{\pi})$. For the latter, it takes into account the known LO contribution from the coupling of pions to axial currents, and its uncertainty comes from the possible unknown short-range contributions. This unknown short-range contributions is expected to be subleading based on the comparison between the pionless and chiral EFTs. Therefore, we expect the truncation uncertainty of the predictions of relativistic pionless

TABLE II. The Minkowski matrix elements $\mathcal{T}_L^{(M)}$ for the ground-state-to-ground-state and first-excited-state-to-first-excited-state $nn \rightarrow ppee$ transitions at the pion masses $m_\pi = 300, 450, 510,$ and 806 MeV, predicted by the LO relativistic pionless EFT. The finite-volume energies E_0 and E_1 for the ground states and the first excited states are also shown, respectively. The uncertainties are obtained by varying the input data of the two-nucleon binding energies B_{nn} from the LQCD calculations within their margins of errors.

m_π (MeV)	L (fm)	E_0 (MeV)	$\mathcal{T}_L^{(M)}(E_0, E_0)$ (MeV ⁵)	E_1 (MeV)	$\mathcal{T}_L^{(M)}(E_1, E_1)$ (MeV ⁵)
300	4	-16.8 ^(+1.3) _(-0.7)	4.1 ^(+0.2) _(-0.1) $\times 10^6$	31.6 ^(+0.9) _(-1.5)	1.9 ^(+0.1) _(-0.2) $\times 10^8$
	5	-12.9 ^(+1.3) _(-0.7)	2.5 ^(+0.2) _(-0.1) $\times 10^6$	17.3 ^(+0.7) _(-1.2)	1.8 ^(+0.1) _(-0.2) $\times 10^8$
	6	-10.8 ^(+1.4) _(-0.7)	1.7 ^(+0.1) _(-0.1) $\times 10^6$	10.2 ^(+0.5) _(-0.9)	1.6 ^(+0.2) _(-0.3) $\times 10^8$
450	4	-18.6 ^(+2.3) _(-2.3)	6.6 ^(+0.5) _(-0.6) $\times 10^6$	23.7 ^(+2.2) _(-1.7)	2.3 ^(+0.4) _(-0.3) $\times 10^8$
	5	-15.5 ^(+2.5) _(-2.4)	4.1 ^(+0.3) _(-0.4) $\times 10^6$	11.4 ^(+1.5) _(-1.2)	1.7 ^(+0.4) _(-0.4) $\times 10^8$
	6	-14.1 ^(+2.6) _(-2.6)	2.8 ^(+0.2) _(-0.3) $\times 10^6$	6.3 ^(+1.1) _(-0.7)	1.2 ^(+0.5) _(-0.3) $\times 10^8$
510	4	-13.7 ^(+1.0) _(-1.0)	6.1 ^(+0.4) _(-0.4) $\times 10^6$	24.2 ^(+1.3) _(-1.2)	3.0 ^(+0.2) _(-0.2) $\times 10^8$
	5	-10.6 ^(+1.1) _(-1.0)	3.7 ^(+0.3) _(-0.3) $\times 10^6$	13.1 ^(+1.0) _(-0.9)	2.5 ^(+0.3) _(-0.3) $\times 10^8$
	6	-9.0 ^(+1.2) _(-1.1)	2.5 ^(+0.2) _(-0.2) $\times 10^6$	7.7 ^(+0.8) _(-0.7)	2.0 ^(+0.4) _(-0.3) $\times 10^8$
806	4	-18.6 ^(+3.0) _(-3.2)	1.2 ^(+0.1) _(-0.1) $\times 10^7$	13.1 ^(+1.8) _(-1.4)	2.6 ^(+0.6) _(-0.5) $\times 10^8$
	5	-16.7 ^(+3.3) _(-3.5)	7.2 ^(+0.6) _(-0.8) $\times 10^6$	6.3 ^(+1.1) _(-0.8)	1.6 ^(+0.7) _(-0.5) $\times 10^8$
	6	-16.0 ^(+3.5) _(-3.6)	4.6 ^(+0.3) _(-0.4) $\times 10^6$	3.4 ^(+0.7) _(-0.5)	9.3 ^(+0.6) _(-0.4) $\times 10^8$

EFT is of the order of $O(Q/m_\pi)$, with Q estimated by the two-nucleon binding energy $\sqrt{m_N B_{nn}}$ or the inverse scattering length a^{-1} . For $m_\pi = 300, 450, 510,$ and 806 MeV, the truncation uncertainties are expected to be of the order of 32%, 28%, 19%, and 20%, respectively. In general, the truncation uncertainty should become smaller for heavier pion mass for the relativistic pionless EFT.

Finally, we present a comparison with the first evaluation of the ground-state-to-ground-state $nn \rightarrow ppee$ matrix element on the lattice with $L = 4.6$ fm at $m_\pi = 806$ MeV, achieved by NPLQCD Collaboration [58]. For the 1S_0 two-nucleon energy at this pion mass, there exists a discrepancy between the older results [74, 98, 99] and the latest result [77] by NPLQCD Collaboration. Such discrepancy is suspected to be due to the misidentification

of the two-nucleon spectrum through “false plateaus” in the older works, yielding a deeply bound two-nucleon state [49, 50, 96]. Several newer works [77, 84–86] have not identified such deeply bound two-nucleon state. Nevertheless, there are several explanations and this issue is still not completely settled [49, 50, 96]. Here, we used both the older and the latest results for the two-nucleon energy from Refs. [74, 77] as inputs of the EFT (Table I), as they are both consistent with the one yielded in the $nn \rightarrow ppee$ calculation [58]. The results are shown below,

$$\begin{aligned} \left| \mathcal{T}_L^{(M)} \right|_{\text{EFT}} &= \begin{cases} 8.7 \begin{smallmatrix} +0.7 \\ -1.0 \end{smallmatrix} \times 10^6 \text{ MeV}^5 & (B_{nn} \simeq 17 \text{ MeV}) \\ 1.7 \begin{smallmatrix} +0.7 \\ -0.4 \end{smallmatrix} \times 10^6 \text{ MeV}^5 & (B_{nn} \simeq 3 \text{ MeV}) \end{cases}, \\ \left| \mathcal{T}_L^{(M)} \right|_{\text{LQCD}} &= 1.75 \begin{smallmatrix} +0.36 \\ -0.36 \end{smallmatrix} \times 10^6 \text{ MeV}^5. \end{aligned} \quad (38)$$

If the latest results of the two-nucleon energy [77] is adopted, the EFT prediction of the matrix element is consistent with the LQCD result, within the uncertainty coming from the inputs. However, if the deeply bound two-nucleon energy from the older calculation [74] is adopted, the matrix element is significantly larger than the LQCD result. This is because the neutrino exchange potential behaves as $1/r$ in the coordinate space, and the larger the binding energy, the more compact the two-nucleon system. In addition, the physical value of the axial coupling constant $g_A = 1.27$ is used here, while g_A should slightly decrease with increasing pion mass [100] and this could slightly decrease the present EFT prediction. Nevertheless, the agreement between the present EFT prediction (using the newest results of the two-nucleon energy [77]) and the first LQCD evaluation for the $nn \rightarrow ppee$ matrix element is very encouraging. To be more conclusive, future benchmarks should be carried out after the LQCD calculations reduce the uncertainties in the two-nucleon energy. In addition, we anticipate more LQCD calculations of the $nn \rightarrow ppee$ matrix elements at different pion masses or finite volumes. Then, the systematic comparison between the EFT matrix elements and the LQCD ones could be a stringent benchmark for the validity of EFT predictions on the $nn \rightarrow ppee$ process.

V. SUMMARY

In this work, the neutrinoless double-beta decay process $nn \rightarrow ppee$ within the light Majorana-neutrino exchange scenario is studied in a finite volume based on the leading-order

relativistic pionless EFT. The finite-volume Minkowski matrix elements of the $nn \rightarrow ppee$ process are predicted for the pion masses $m_\pi = 300, 450, 510,$ and 806 MeV, at which the LQCD calculations of the two-nucleon energies exist. These results can be directly compared to the results from LQCD calculations of the $nn \rightarrow ppee$ process at the same pion masses.

The previous studies [59, 60] presented the matching framework between the finite-volume matrix elements from LQCD and the infinite-volume scattering amplitude from the nonrelativistic pionless EFT for the $nn \rightarrow ppee$ process. The scattering amplitudes and finite-volume Minkowski matrix elements of the $nn \rightarrow ppee$ process are calculated at the physical pion masses [60], where the size of the LO $nn \rightarrow ppee$ contact term is determined by the generalized Cottingham formula [31]. However, such determination of the contact term is not applicable at the unphysical pion masses. Different from the nonrelativistic studies, the present work presents a relativistic study, where the size of the contact term is determined by integrating out the pion contributions to the long-range neutrino potential in the relativistic chiral EFT. This is possible thanks to the fact that the long-range $nn \rightarrow ppee$ amplitudes are renormalizable at leading order in the relativistic chiral EFT [33], in contrast to the nonrelativistic case. The obtained amplitudes at the physical pion mass are consistent with the previous nonrelativistic results at 20% level. In addition, the $nn \rightarrow ppee$ processes at the unphysical pion masses $m_\pi = 300, 450, 510,$ and 806 MeV are studied in a finite volume for the first time, based on the relativistic pionless EFT, using the two-nucleon energies from the existing LQCD calculations [73–77].

At the unphysical pion masses, the renormalization-group invariance of the leading-order Minkowski matrix elements is confirmed. Then, the matrix elements are predicted in several different volumes to investigate their volume dependence. It is found that a much larger volume than those implemented in the present LQCD studies of two-nucleon systems (typically with cubic-box sizes in the range of $L = 4-6$ fm) is required to approach the infinite-volume limits of the $nn \rightarrow ppee$ matrix elements, due to the long-range nature of neutrino exchange. The finite-volume results can be improved by the extrapolation considering the leading $O(1/L)$ correction, but systematic deviations from the infinite-volume limit remain for about 10%-20%, depending on the pion mass.

Finally, the relativistic pionless EFT predictions of the Minkowski matrix elements in several finite volumes are presented for the ground-state-to-ground-state and first-excited-state-to-first-excited-state $nn \rightarrow ppee$ transitions at the pion masses $m_\pi = 300, 450, 510,$ and

806 MeV. These results allow direct benchmarks between EFT and LQCD on the $nn \rightarrow ppee$ process, especially at the heavy pion masses that are numerically more favorable for LQCD. In particular, the EFT predictions for $m_\pi = 806$ MeV are compared with the first LQCD evaluation of the ground-state-to-ground-state $nn \rightarrow ppee$ matrix element at a finite volume of $L = 4.6$ fm [58]. Using the latest LQCD value of two-nucleon energy in a same lattice setup [77] as inputs, the relativistic pionless EFT yields a $nn \rightarrow ppee$ matrix element in good agreement with the LQCD evaluation. This is not the case if the deeply bound two-nucleon energy from the older LQCD calculation [74] is used.

The present results motivate future studies of the $nn \rightarrow ppee$ process from LQCD at different pion masses and finite volumes. In addition, the present leading-order study on the $nn \rightarrow ppee$ process in a finite volume also provides the basis for such studies at higher orders, where the LECs associated with subleading lepton-number-breaking contact terms have to be determined via matching to LQCD calculations.

ACKNOWLEDGMENTS

This work has been supported in part by the National Natural Science Foundation of China (Grants No. 123B2080, No. 12141501, No. 11935003), and the High-performance Computing Platform of Peking University. We acknowledge the funding support from the State Key Laboratory of Nuclear Physics and Technology, Peking University (Grant No. NPT2023ZX03).

-
- [1] W. H. Furry, On Transition Probabilities in Double Beta-Disintegration, *Phys. Rev.* **56**, 1184 (1939).
 - [2] J. Schechter and J. W. F. Valle, Neutrinoless double- β decay in $SU(2) \times U(1)$ theories, *Phys. Rev. D* **25**, 2951 (1982).
 - [3] Y. B. Zel'dovich and M. Y. Khlopov, Study of the neutrino mass in a double beta-decay, *JETP Lett.* **34**, 141 (1981).
 - [4] C. E. Aalseth *et al.* (Majorana Collaboration), Search for Neutrinoless Double- β Decay in ^{76}Ge with the Majorana Demonstrator, *Phys. Rev. Lett.* **120**, 132502 (2018).

- [5] D. Q. Adams *et al.* (CUORE Collaboration), Improved Limit on Neutrinoless Double-Beta Decay in ^{130}Te with CUORE, *Phys. Rev. Lett.* **124**, 122501 (2020).
- [6] M. Agostini *et al.* (GERDA Collaboration), Final Results of GERDA on the Search for Neutrinoless Double- β Decay, *Phys. Rev. Lett.* **125**, 252502 (2020).
- [7] J. B. Albert *et al.* (EXO-200 Collaboration), Search for Neutrinoless Double-Beta Decay with the Upgraded EXO-200 Detector, *Phys. Rev. Lett.* **120**, 072701 (2018).
- [8] E. Armengaud *et al.* (CUPID-Mo Collaboration), New Limit for Neutrinoless Double-Beta Decay of ^{100}Mo from the CUPID-Mo Experiment, *Phys. Rev. Lett.* **126**, 181802 (2021).
- [9] R. Arnold *et al.* (NEMO-3 Collaboration), Search for Neutrinoless Quadruple- β Decay of ^{150}Nd with the NEMO-3 Detector, *Phys. Rev. Lett.* **119**, 041801 (2017).
- [10] A. Gando *et al.* (KamLAND-Zen Collaboration), Search for Majorana Neutrinos Near the Inverted Mass Hierarchy Region with KamLAND-Zen, *Phys. Rev. Lett.* **117**, 082503 (2016).
- [11] W. H. Dai *et al.* (CDEX Collaboration), Search for neutrinoless double-beta decay of ^{76}Ge with a natural broad energy germanium detector, *Phys. Rev. D* **106**, 032012 (2022).
- [12] M. Agostini, G. Benato, J. A. Detwiler, J. Menéndez, and F. Vissani, Toward the discovery of matter creation with neutrinoless $\beta\beta$ decay, *Rev. Mod. Phys.* **95**, 025002 (2023).
- [13] J. Engel and J. Menéndez, Status and future of nuclear matrix elements for neutrinoless double-beta decay: a review, *Rep. Prog. Phys.* **80**, 046301 (2017).
- [14] S. Weinberg, Nuclear forces from chiral lagrangians, *Phys. Lett. B* **251**, 288 (1990).
- [15] S. Weinberg, Effective chiral lagrangians for nucleon-pion interactions and nuclear forces, *Nucl. Phys. B* **363**, 3 (1991).
- [16] D. B. Kaplan, M. J. Savage, and M. B. Wise, A new expansion for nucleon-nucleon interactions, *Phys. Lett. B* **424**, 390 (1998).
- [17] D. B. Kaplan, M. J. Savage, and M. B. Wise, Two-nucleon systems from effective field theory, *Nucl. Phys. B* **534**, 329 (1998).
- [18] U. van Kolck, Effective field theory of short-range forces, *Nucl. Phys. A* **645**, 273 (1999).
- [19] P. Bedaque and U. van Kolck, Nucleon-deuteron scattering from an effective field theory, *Phys. Lett. B* **428**, 221 (1998).
- [20] P. F. Bedaque, H.-W. Hammer, and U. van Kolck, Effective theory for neutron-deuteron scattering: Energy dependence, *Phys. Rev. C* **58**, R641 (1998).
- [21] J.-W. Chen, G. Rupak, and M. J. Savage, Nucleon-nucleon effective field theory without

- pions, Nucl. Phys. A **653**, 386 (1999).
- [22] E. Epelbaum, H.-W. Hammer, and U.-G. Meißner, Modern theory of nuclear forces, Rev. Mod. Phys. **81**, 1773 (2009).
- [23] R. Machleidt and D. R. Entem, Chiral effective field theory and nuclear forces, Phys. Rep. **503**, 1 (2011).
- [24] H.-W. Hammer, S. König, and U. van Kolck, Nuclear effective field theory: Status and perspectives, Rev. Mod. Phys. **92**, 025004 (2020).
- [25] G. Prézeau, M. Ramsey-Musolf, and P. Vogel, Neutrinoless double β decay and effective field theory, Phys. Rev. D **68**, 034016 (2003).
- [26] V. Cirigliano, W. Dekens, J. de Vries, M. L. Graesser, and E. Mereghetti, Neutrinoless double beta decay in chiral effective field theory: lepton number violation at dimension seven, J. High Energy Phys. **2017** (12), 82.
- [27] V. Cirigliano, W. Dekens, E. Mereghetti, and A. Walker-Loud, Neutrinoless double- β decay in effective field theory: The light-Majorana neutrino-exchange mechanism, Phys. Rev. C **97**, 065501 (2018).
- [28] V. Cirigliano, W. Dekens, J. de Vries, M. L. Graesser, E. Mereghetti, S. Pastore, and U. van Kolck, New Leading Contribution to Neutrinoless Double- β Decay, Phys. Rev. Lett. **120**, 202001 (2018).
- [29] V. Cirigliano, W. Dekens, J. de Vries, M. L. Graesser, E. Mereghetti, S. Pastore, M. Piarulli, U. van Kolck, and R. B. Wiringa, Renormalized approach to neutrinoless double- β decay, Phys. Rev. C **100**, 055504 (2019).
- [30] W. Dekens, J. de Vries, K. Fuyuto, E. Mereghetti, and G. Zhou, Sterile neutrinos and neutrinoless double beta decay in effective field theory, J. High Energy Phys. **2020** (6), 97.
- [31] V. Cirigliano, W. Dekens, J. de Vries, M. Hoferichter, and E. Mereghetti, Toward Complete Leading-Order Predictions for Neutrinoless Double β Decay, Phys. Rev. Lett. **126**, 172002 (2021).
- [32] V. Cirigliano, W. Dekens, J. de Vries, M. Hoferichter, and E. Mereghetti, Determining the leading-order contact term in neutrinoless double β decay, J. High Energy Phys. **2021** (5), 289.
- [33] Y. Yang and P. Zhao, Relativistic model-free prediction for neutrinoless double beta decay at leading order, Phys. Lett. B **855**, 138782 (2024).

- [34] J. Menéndez, D. Gazit, and A. Schwenk, Chiral Two-Body Currents in Nuclei: Gamow-Teller Transitions and Neutrinoless Double-Beta Decay, *Phys. Rev. Lett.* **107**, 062501 (2011).
- [35] S. Pastore, J. Carlson, V. Cirigliano, W. Dekens, E. Mereghetti, and R. B. Wiringa, Neutrinoless double- β decay matrix elements in light nuclei, *Phys. Rev. C* **97**, 014606 (2018).
- [36] L.-J. Wang, J. Engel, and J. M. Yao, Quenching of nuclear matrix elements for $0\nu\beta\beta$ decay by chiral two-body currents, *Phys. Rev. C* **98**, 031301 (2018).
- [37] L. Jokiniemi, P. Soriano, and J. Menéndez, Impact of the leading-order short-range nuclear matrix element on the neutrinoless double-beta decay of medium-mass and heavy nuclei, *Phys. Lett. B* **823**, 136720 (2021).
- [38] J. M. Yao, A. Belley, R. Wirth, T. Miyagi, C. G. Payne, S. R. Stroberg, H. Hergert, and J. D. Holt, Ab initio benchmarks of neutrinoless double- β decay in light nuclei with a chiral Hamiltonian, *Phys. Rev. C* **103**, 014315 (2021).
- [39] R. Weiss, P. Soriano, A. Lovato, J. Menendez, and R. B. Wiringa, Neutrinoless double- β decay: Combining quantum Monte Carlo and the nuclear shell model with the generalized contact formalism, *Phys. Rev. C* **106**, 065501 (2022).
- [40] A. Belley, J. M. Yao, B. Bally, J. Pitcher, J. Engel, H. Hergert, J. D. Holt, T. Miyagi, T. R. Rodríguez, A. M. Romero, S. R. Stroberg, and X. Zhang, Ab Initio Uncertainty Quantification of Neutrinoless Double-Beta Decay in ^{76}Ge , *Phys. Rev. Lett.* **132**, 182502 (2024).
- [41] S. Weinberg, Baryon- and Lepton-Nonconserving Processes, *Phys. Rev. Lett.* **43**, 1566 (1979).
- [42] E. Epelbaum and J. Gegelia, Weinberg’s approach to nucleon-nucleon scattering revisited, *Phys. Lett. B* **716**, 338 (2012).
- [43] E. Epelbaum, J. Gegelia, U.-G. Meißner, and D.-L. Yao, Renormalization of the three-boson system with short-range interactions revisited, *Eur. Phys. J. A* **53**, 98 (2017).
- [44] Y. L. Yang and P. W. Zhao, A consistent description of the relativistic effects and three-body interactions in atomic nuclei, *Phys. Lett. B* **835**, 137587 (2022).
- [45] R. A. Briceño, Z. Davoudi, and T. C. Luu, Nuclear reactions from lattice QCD, *J. Phys. G* **42**, 023101 (2015).
- [46] V. Cirigliano, Z. Davoudi, T. Bhattacharya, T. Izubuchi, P. E. Shanahan, S. Syritsyn, M. L. Wagman, and U. S. Q. C. D. Collaboration, The role of Lattice QCD in searches for violations of fundamental symmetries and signals for new physics, *Eur. Phys. J. A* **55**, 197 (2019).

- [47] A. S. Kronfeld, D. G. Richards, W. Detmold, R. Gupta, H.-W. Lin, K.-F. Liu, A. S. Meyer, R. Sufian, and S. Syritsyn, Lattice QCD and neutrino-nucleus scattering, *Eur. Phys. J. A* **55**, 196 (2019).
- [48] V. Cirigliano, W. Detmold, A. Nicholson, and P. Shanahan, Lattice QCD Inputs for nuclear double beta decay, *Prog. Part. Nucl. Phys.* **112**, 103771 (2020).
- [49] C. Drischler, W. Haxton, K. McElvain, E. Mereghetti, A. Nicholson, P. Vranas, and A. Walker-Loud, Towards grounding nuclear physics in QCD, *Prog. Part. Nucl. Phys.* **121**, 103888 (2021).
- [50] Z. Davoudi, W. Detmold, P. Shanahan, K. Orginos, A. Parreño, M. J. Savage, and M. L. Wagman, Nuclear matrix elements from lattice QCD for electroweak and beyond-Standard-Model processes, *Phys. Rep.* **900**, 1 (2021).
- [51] V. Cirigliano, Z. Davoudi, J. Engel, R. J. Furnstahl, G. Hagen, U. Heinz, H. Hergert, M. Horoi, C. W. Johnson, A. Lovato, E. Mereghetti, W. Nazarewicz, A. Nicholson, T. Papenbrock, S. Pastore, M. Plumlee, D. R. Phillips, P. E. Shanahan, S. R. Stroberg, F. Viens, A. Walker-Loud, K. A. Wendt, and S. M. Wild, Towards precise and accurate calculations of neutrinoless double-beta decay, *J. Phys. G* **49**, 120502 (2022).
- [52] X. Feng, L.-C. Jin, X.-Y. Tuo, and S.-C. Xia, Light-Neutrino Exchange and Long-Distance Contributions to $0\nu 2\beta$ Decays: An Exploratory Study on $\pi\pi \rightarrow ee$, *Phys. Rev. Lett.* **122**, 022001 (2019).
- [53] X.-Y. Tuo, X. Feng, and L.-C. Jin, Long-distance contributions to neutrinoless double beta decay $\pi^- \rightarrow \pi^+ ee$, *Phys. Rev. D* **100**, 094511 (2019).
- [54] W. Detmold and D. J. Murphy, Neutrinoless double beta decay from lattice QCD: The long-distance $\pi^- \rightarrow \pi^+ e^- e^-$ amplitude, arXiv:2004.07404 (2020).
- [55] A. Nicholson, E. Berkowitz, H. Monge-Camacho, D. Brantley, N. Garron, C. C. Chang, E. Rinaldi, M. A. Clark, B. Joó, T. Kurth, B. C. Tiburzi, P. Vranas, and A. Walker-Loud, Heavy physics contributions to neutrinoless double beta decay from qcd, *Phys. Rev. Lett.* **121**, 172501 (2018).
- [56] P. E. Shanahan, B. C. Tiburzi, M. L. Wagman, F. Winter, E. Chang, Z. Davoudi, W. Detmold, K. Orginos, and M. J. Savage (NPLQCD Collaboration), Isotensor Axial Polarizability and Lattice QCD Input for Nuclear Double- β Decay Phenomenology, *Phys. Rev. Lett.* **119**, 062003 (2017).

- [57] B. C. Tiburzi, M. L. Wagman, F. Winter, E. Chang, Z. Davoudi, W. Detmold, K. Orginos, M. J. Savage, and P. E. Shanahan (NPLQCD Collaboration), Double- β decay matrix elements from lattice quantum chromodynamics, *Phys. Rev. D* **96**, 054505 (2017).
- [58] Z. Davoudi, W. Detmold, Z. Fu, A. V. Grebe, W. Jay, D. Murphy, P. Oare, P. E. Shanahan, and M. L. Wagman (NPLQCD Collaboration), Long-distance nuclear matrix elements for neutrinoless double-beta decay from lattice QCD, *Phys. Rev. D* **109**, 114514 (2024).
- [59] Z. Davoudi and S. V. Kadam, Path from Lattice QCD to the Short-Distance Contribution to $0\nu\beta\beta$ Decay with a Light Majorana Neutrino, *Phys. Rev. Lett.* **126**, 152003 (2021).
- [60] Z. Davoudi and S. V. Kadam, Extraction of low-energy constants of single- and double- β decays from lattice QCD: A sensitivity analysis, *Phys. Rev. D* **105**, 094502 (2022).
- [61] L. Lellouch and M. Lüscher, Weak transition matrix elements from finite-volume correlation functions, *Commun. Math. Phys.* **219**, 31 (2001).
- [62] W. Detmold and M. J. Savage, Electroweak matrix elements in the two-nucleon sector from lattice QCD, *Nucl. Phys. A* **743**, 170 (2004).
- [63] H. B. Meyer, Lattice QCD and the Timelike Pion Form Factor, *Phys. Rev. Lett.* **107**, 072002 (2011).
- [64] R. A. Briceño and Z. Davoudi, Moving multichannel systems in a finite volume with application to proton-proton fusion, *Phys. Rev. D* **88**, 094507 (2013).
- [65] V. Bernard, D. Hoja, U.-G. Meißner, and A. Rusetsky, Matrix elements of unstable states, *J. High Energy Phys.* **2012** (9), 23.
- [66] R. A. Briceño, M. T. Hansen, and A. Walker-Loud, Multichannel $1 \rightarrow 2$ transition amplitudes in a finite volume, *Phys. Rev. D* **91**, 034501 (2015).
- [67] R. A. Briceño and M. T. Hansen, Multichannel $0 \rightarrow 2$ and $1 \rightarrow 2$ transition amplitudes for arbitrary spin particles in a finite volume, *Phys. Rev. D* **92**, 074509 (2015).
- [68] R. A. Briceño and M. T. Hansen, Relativistic, model-independent, multichannel $2 \rightarrow 2$ transition amplitudes in a finite volume, *Phys. Rev. D* **94**, 013008 (2016).
- [69] N. H. Christ, X. Feng, G. Martinelli, and C. T. Sachrajda, Effects of finite volume on the $K_L - K_S$ mass difference, *Phys. Rev. D* **91**, 114510 (2015).
- [70] R. A. Briceño, Z. Davoudi, M. T. Hansen, M. R. Schindler, and A. Baroni, Long-range electroweak amplitudes of single hadrons from Euclidean finite-volume correlation functions, *Phys. Rev. D* **101**, 014509 (2020).

- [71] X. Feng, L.-C. Jin, Z.-Y. Wang, and Z. Zhang, Finite-volume formalism in the $2 \xrightarrow{H_I+H_I}$ transition: An application to the lattice QCD calculation of double beta decays, *Phys. Rev. D* **103**, 034508 (2021).
- [72] Z. Davoudi and S. V. Kadam, Two-neutrino double- β decay in pionless effective field theory from a Euclidean finite-volume correlation function, *Phys. Rev. D* **102**, 114521 (2020).
- [73] T. Yamazaki, K.-i. Ishikawa, Y. Kuramashi, and A. Ukawa, Helium nuclei, deuteron, and dineutron in 2+1 flavor lattice qcd, *Phys. Rev. D* **86**, 074514 (2012).
- [74] S. R. Beane, E. Chang, S. D. Cohen, W. Detmold, H. W. Lin, T. C. Luu, K. Orginos, A. Parreño, M. J. Savage, and A. Walker-Loud (NPLQCD Collaboration), Light nuclei and hypernuclei from quantum chromodynamics in the limit of SU(3) flavor symmetry, *Phys. Rev. D* **87**, 034506 (2013).
- [75] T. Yamazaki, K.-i. Ishikawa, Y. Kuramashi, and A. Ukawa, Study of quark mass dependence of binding energy for light nuclei in 2+1 flavor lattice QCD, *Phys. Rev. D* **92**, 014501 (2015).
- [76] M. Illa, S. R. Beane, E. Chang, Z. Davoudi, W. Detmold, D. J. Murphy, K. Orginos, A. Parreño, M. J. Savage, P. E. Shanahan, M. L. Wagman, and F. Winter (NPLQCD Collaboration), Low-energy scattering and effective interactions of two baryons at $m_\pi \sim 450$ MeV from lattice quantum chromodynamics, *Phys. Rev. D* **103**, 054508 (2021).
- [77] S. Amarasinghe, R. Baghdadi, Z. Davoudi, W. Detmold, M. Illa, A. Parreño, A. V. Pochinsky, P. E. Shanahan, and M. L. Wagman, Variational study of two-nucleon systems with lattice QCD, *Phys. Rev. D* **107**, 094508 (2023).
- [78] N. Cabibbo, Unitary Symmetry and Leptonic Decays, *Phys. Rev. Lett.* **10**, 531 (1963).
- [79] M. Kobayashi and T. Maskawa, CP-Violation in the Renormalizable Theory of Weak Interaction, *Prog. Theor. Phys.* **49**, 652 (1973).
- [80] Y. Xiao, L.-S. Geng, and X.-L. Ren, Covariant nucleon-nucleon contact Lagrangian up to order $\mathcal{O}(q^4)$, *Phys. Rev. C* **99**, 024004 (2019).
- [81] P. F. Bedaque and U. van Kolck, EFFECTIVE FIELD THEORY FOR FEW-NUCLEON SYSTEMS*, *Ann. Rev. Nucl. Part. Sci.* **52**, 339 (2002).
- [82] M. Lüscher, Volume dependence of the energy spectrum in massive quantum field theories, *Commun. Math. Phys.* **105**, 153 (1986).
- [83] M. Lüscher, Two-particle states on a torus and their relation to the scattering matrix,

- Nucl. Phys. B **354**, 531 (1991).
- [84] A. Francis, J. R. Green, P. M. Junnarkar, C. Miao, T. D. Rae, and H. Wittig, Lattice QCD study of the H dibaryon using hexaquark and two-baryon interpolators, Phys. Rev. D **99**, 074505 (2019).
- [85] B. Hörz, D. Howarth, E. Rinaldi, A. Hanlon, C. C. Chang, C. Körber, E. Berkowitz, J. Bulava, M. A. Clark, W. T. Lee, C. Morningstar, A. Nicholson, P. Vranas, and A. Walker-Loud, Two-nucleon S -wave interactions at the SU(3) flavor-symmetric point with $m_{ud} \approx m_s^{\text{phys}}$: A first lattice QCD calculation with the stochastic Laplacian Heaviside method, Phys. Rev. C **103**, 014003 (2021).
- [86] W. Detmold, M. Illa, W. I. Jay, A. Parreño, R. J. Perry, P. E. Shanahan, and M. L. Wagman, Constraints on the finite volume two-nucleon spectrum at $m_\pi \simeq 806$ MeV, arXiv:2404.12039 (2024).
- [87] W. Glöckle, *The Quantum Mechanical Few-Body Problem*, edited by W. Beiglböck, E. H. Lieb, T. Regge, and W. Thirring (Springer-Verlag Berlin, 1983).
- [88] Y. R. Kwon and F. Tabakin, Hadronic atoms in momentum space, Phys. Rev. C **18**, 932 (1978).
- [89] R. H. Landau, Coupled bound and continuum eigenstates in momentum space, Phys. Rev. C **27**, 2191 (1983).
- [90] Lande, private communication in Refs. [89] and [88], .
- [91] I. Ivanov and J. Mitroy, Treatment of the Coulomb singularity in momentum space calculations, Comp. Phys. Commun. **134**, 317 (2001).
- [92] S. Tan, Three-boson problem at low energy and implications for dilute bose-einstein condensates, Phys. Rev. A **78**, 013636 (2008).
- [93] S. R. Beane and M. J. Savage, Two-particle elastic scattering in a finite volume including QED, Phys. Rev. D **90**, 074511 (2014).
- [94] N. Ishii, S. Aoki, T. Doi, T. Hatsuda, Y. Ikeda, T. Inoue, K. Murano, H. Nemura, and K. Sasaki, Hadron-hadron interactions from imaginary-time Nambu-Bethe-Salpeter wave function on the lattice, Phys. Lett. B **712**, 437 (2012).
- [95] T. Inoue, S. Aoki, T. Doi, T. Hatsuda, Y. Ikeda, N. Ishii, K. Murano, H. Nemura, and K. Sasaki, Two-baryon potentials and H-dibaryon from 3-flavor lattice QCD simulations, Nucl. Phys. A **881**, 28 (2012), progress in Strangeness Nuclear Physics.

- [96] I. Tews, Z. Davoudi, A. Ekström, J. D. Holt, K. Becker, R. Briceño, D. J. Dean, W. Detmold, C. Drischler, T. Duguet, E. Epelbaum, A. Gasparyan, J. Gegelia, J. R. Green, H. W. Griebhammer, A. D. Hanlon, M. Heinz, H. Hergert, M. Hoferichter, M. Illa, D. Kekejian, A. Kievsky, S. König, H. Krebs, K. D. Launey, D. Lee, P. Navrátil, A. Nicholson, A. Parreño, D. R. Phillips, M. Płoszajczak, X.-L. Ren, T. R. Richardson, C. Robin, G. H. Sargsyan, M. J. Savage, M. R. Schindler, P. E. Shanahan, R. P. Springer, A. Tichai, U. v. Kolck, M. L. Wagman, A. Walker-Loud, C.-J. Yang, and X. Zhang, *Nuclear Forces for Precision Nuclear Physics: A Collection of Perspectives, Few-Body Systems* **63**, 67 (2022).
- [97] Z. Davoudi and M. J. Savage, Finite-volume electromagnetic corrections to the masses of mesons, baryons, and nuclei, *Phys. Rev. D* **90**, 054503 (2014).
- [98] E. Berkowitz, T. Kurth, A. Nicholson, B. Joó, E. Rinaldi, M. Strother, P. M. Vranas, and A. Walker-Loud, Two-nucleon higher partial-wave scattering from lattice QCD, *Physics Letters B* **765**, 285 (2017).
- [99] M. L. Wagman, F. Winter, E. Chang, Z. Davoudi, W. Detmold, K. Orginos, M. J. Savage, and P. E. Shanahan (NPLQCD Collaboration), Baryon-baryon interactions and spin-flavor symmetry from lattice quantum chromodynamics, *Phys. Rev. D* **96**, 114510 (2017).
- [100] C. C. Chang, A. N. Nicholson, E. Rinaldi, E. Berkowitz, N. Garron, D. A. Brantley, H. Monge-Camacho, C. J. Monahan, C. Bouchard, M. A. Clark, B. Joó, T. Kurth, K. Orginos, P. Vranas, and A. Walker-Loud, A per-cent-level determination of the nucleon axial coupling from quantum chromodynamics, *Nature* **558**, 91 (2018).